Research Square

Preprints are preliminary reports that have not undergone peer review.
They should not be considered conclusive, used to inform clinical practice,
or referenced by the media as validated information.

# A plant virus, TYLCV, up-regulates an endocrine oxylipin signal in its insect vector, Bemisia tabaci, via the viral C2 virulence factor for viral transmission

**Niayesh Shahmohammadi**
Gyeongkuk National University
**Tae-Geun Song**
Gyeongkuk National University
**Man-Cheol Son**
Gyeongkuk National University
**Jiho Jeon**
Gyeongkuk National University
**Donghee Lee**
Gyeongkuk National University
**Eui-Joon Kil**
Gyeongkuk National University
**Yonggyun Kim**
hosanna@gknu.ac.kr

Gyeongkuk National University

**Research Article**

**Keywords:** Bemisia tabaci, TYLCV, EpOME, eicosanoid, apoptosis, immune response

**Posted Date:** June 9th, 2026

**DOI:** https://doi.org/10.21203/rs.3.rs-9891096/v1

**License:** This work is licensed under a Creative Commons Attribution 4.0 International License.
Read Full License

**Additional Declarations:** No competing interests reported.

**Virology Journal**

# A plant virus, TYLCV, up-regulates an endocrine oxylipin signal in its insect vector, *Bemisia tabaci*, via the viral C2 virulence factor for viral transmission

**Niayesh Shahmohammadi, Tae-Geun Song, Man-Cheol Son, Jiho Jeon, Donghee Lee, Eui-Joon Kil and Yonggyun Kim***

*School of Life Science & Engineering, Gyeongkuk National University, Andong 36729, Korea*

* Corresponding author: hosanna@gknu.ac.kr

**Abstract**

**Background** Tomato yellow leaf curl virus (TYLCV) is transmitted by *Bemisia tabaci* through a circulative and replicative pathway and must overcome vector immune defenses to achieve efficient transmission. Oxylipins are important regulators of insect immunity, in which eicosanoids generally promote antiviral responses whereas C18 epoxyoctadecamonoenoic acids (EpOMEs) act as immune suppressors. Although manipulation of insect immunity by plant viruses has been increasingly recognized, the molecular mechanisms by which TYLCV reshapes vector physiology to establish a permissive infection state remain poorly understood.

**Methodology** TYLCV infection and localization in *B. tabaci* were analyzed using fluorescence in situ hybridization (FISH), immunofluorescence assays (IFA), and quantitative PCR. Oxylipin functions were examined through oral delivery of prostaglandins, EpOMEs, pathway inhibitors, and lipid analogs. EpOME levels were quantified by LC–MS/MS. Candidate genes involved in eicosanoid and EpOME biosynthesis or degradation were predicted through bioinformatic and phylogenetic analyses and functionally evaluated using RNA interference (RNAi). Intestinal apoptosis was assessed using TUNEL and cleaved caspase-3 immunostaining. Immune-associated genes and viral determinants were investigated through RT-qPCR and gene-specific RNAi, including silencing of all six TYLCV genes.

**Results** TYLCV progressively accumulated in the intestine of *B. tabaci* and significantly altered fatty acid metabolism. Two oxylipin pathways exerted antagonistic effects on viral accumulation. Prostaglandin $E_2$ ($PGE_2$) and its biosynthetic machinery, including BtPLA2-A, BtPLA2-C, Bt-PGES2, and Bt-PGE2R, functioned as antiviral regulators, whereas both EpOME isomers (9,10- and 12,13-EpOME) promoted viral accumulation. TYLCV infection elevated EpOME levels more than two-fold and transcriptionally favored EpOME accumulation by inducing *Bt-CYP6* while suppressing *Bt-sEH2* and *Bt-sEH3*. Pharmacological

and RNAi analyses confirmed *Bt-CYP6* as an EpOME-associated synthase and *Bt-sEH2/3* as degradation-associated genes. EpOME promoted intestinal apoptosis and selectively regulated immune-associated genes, inducing proviral factors including defensin and cathepsins while suppressing antiviral factors such as knottin and PGRP. Comparison of TYLCV strains revealed that the more virulent TYLCV-IL induced stronger EpOME signaling and apoptosis than TYLCV-Mld. Among all viral genes, only TYLCV-C2 controlled host EpOME machinery; silencing C2 abolished *Bt-CYP6* induction and restored *Bt-sEH2/3* expression, while exogenous EpOME rescued viral accumulation.

**Conclusion** TYLCV exploits vector oxylipin signaling to establish a permissive physiological state in *B. tabaci*. Through the viral C2 factor, TYLCV shifts host signaling from an antiviral eicosanoid-dominant state toward a proviral EpOME-dominant state, thereby promoting apoptosis, reshaping immune responses, and enhancing viral accumulation and transmission potential.

**Keywords** *Bemisia tabaci*, TYLCV, EpOME, eicosanoid, apoptosis, immune response

## Introduction

The silverleaf whitefly, *Bemisia tabaci* (Gennadius), is an insect pest damaging > 600 plant species by directly feeding and indirectly transmitting plant viruses classified in the genus *Begomovirus* [1, 2]. It is highly invasive and now distributed across most subtropical and temperate regions worldwide, with a cryptic species complex consisting of at least 43 genetically distinct lineages, which are morphologically indistinguishable but can be discriminated by genetic and behavioral traits [3, 4]. Among them, two invasive species, Middle East–Asia Minor 1 (MEAM1 = B biotype) and Mediterranean (MED = Q biotype), are particularly notorious for their ability to transmit plant viruses along with development of insecticide resistance [5, 6].

One of the most important viruses transmitted by *B. tabaci* is tomato yellow leaf curl virus (TYLCV, *Begomovirus coheni*), a member of *Begomovirus* with a single-stranded DNA genome [7]. Phylogenetic studies have identified at least six TYLCV-related viruses, including TYLCV, tomato yellow leaf curl Sardinia virus (TYLCSV), tomato yellow leaf curl Axiarqua virus (TYLCAxV), tomato yellow leaf curl Malaga virus (TYLCMalV), tomato yellow leaf curl Mali virus (TYLCMV), and tomato leaf curl Sudan virus (ToLCSDV) [8]. Among these, TYLCV is the most widespread and emergent species. TYLCV-induced disease is regarded as one of the most devastating plant diseases in temperate regions [9]. Infected plants are less vigorous, yield fruits of reduced market value, and when infected during early growth stages, may experience complete crop loss [9]. The first TYLCV genome was sequenced from Israel (TYLCV-IL) in 1991 [10], followed by the identification of a mild strain, TYLCV-Mld [11]. Based on sequence identity, five major strains have been described, including Gezira (TYLCV-Gez), Iran (TYLCV-IR), Oman (TYLCV-OM), TYLCV-IL, and TYLCV-Mld. Over the past decades, whiteflies and begomoviruses together have emerged as major threats to vegetable

82 production worldwide [12].

83 In response to viral infection, insects mount antiviral immune defenses essential for
84 their survival. Insect immunity is innate and relies on pathogen recognition mechanisms that
85 are genetically pre-programmed [13]. Upon recognition, oxylipins act as key mediators of
86 nonself signaling to modulate immune responses of two effector tissues, such as hemocytes
87 and fat body, which perform cellular and humoral immune responses [14]. Oxylipins are
88 oxygenated derivatives of polyunsaturated fatty acids (PUFAs) and are broadly categorized
89 into two subgroups in insects [15]. Eicosanoids, including prostaglandins (PGs), leukotrienes,
90 and epoxyeicosatrienoic acids, are C20 PUFAs that promote immune responses. Their
91 biosynthesis is typically induced upon pathogenic infection through the activation of
92 phospholipase $A_2$ ($PLA_2$), which liberates arachidonic acid (20:4n-6) and other C20 PUFAs
93 from membrane phospholipids. In contrast, epoxyoctadecamonoenoic acids (EpOMEs),
94 including vernolic acid (12,13-EpOME) and coronaric acid (9,10-EpOME), are C18 oxylipins
95 that act as immune suppressors [16]. They are synthesized by cytochrome P450
96 monooxygenases (CYPs) and degraded by soluble epoxide hydrolase (sEH) in different insect
97 species [17, 18].

98 Pathogens often exploit oxylipin pathways to subvert host immunity. For example, the
99 symbiotic bacteria *Xenorhabdus* and *Photorhabdus*-associated with entomopathogenic
100 nematodes *Steinernema* and *Heterorhabditis*, respectively, produce secondary metabolites such
101 as benzylideneacetone and non-ribosomal peptides that inhibit $PLA_2$ activity, thereby blocking
102 eicosanoid biosynthesis [19, 20]. This suppression prevents the insect host from mounting
103 immune responses, creating an immunocompromised environment that facilitates bacterial
104 proliferation and nematode development within the insect cadaver [21]. Similarly, tomato
105 spotted wilt virus (TSWV) manipulates EpOME metabolism in its thrips vector, *Frankliniella*

*occidentalis*, to antagonize eicosanoid-mediated antiviral responses [22, 23]. Viral infection induces prostaglandin $E_2$ ($PGE_2$) biosynthesis, which mediates apoptosis in the midgut epithelium of thrips larvae and restricts viral replication [24]. However, EpOMEs counteract this antiviral apoptotic response. A viral factor encoded by the NSs gene of TSWV has been shown to upregulate EpOME biosynthesis, thereby promoting viral replication [23]. The proviral role of EpOMEs has also been demonstrated in entomopathogenic baculoviruses [25]. These findings suggest that EpOME biosynthesis may represent a common molecular target exploited by different viral pathogens to suppress insect immunity.

This study was designed to test a hypothesis that TYLCV manipulates EpOME biosynthesis in its insect vector *B. tabaci* to facilitate circulative viral transmission. Specifically, we aimed to identify the biosynthetic machinery underlying the production of the two oxylipins and to evaluate their respective roles in TYLCV transmission.

## Materials and methods

### Rearing *B. tabaci*

A colony of the MED-type whitefly, *B. tabaci*, was originally collected from a greenhouse in Andong, Korea, and was maintained on tomato (*Solanum lycopersicum*) seedlings under controlled laboratory conditions (25 ± 1°C, 14 h light photoperiod and 70 ± 5% relative humidity). The whitefly strain was confirmed by sequencing a cytochrome oxidase I (COI) segment of the whitefly, which was deposited in GenBank under an accession number of PV993946.

### Origin of two TYLCV strains and disease severity index

To obtain virus-infected plants, infectious clones of TYLCV-IL (GenBank accession number:

JN680149) or TYLCV-Mld (GenBank accession number: PX375450) strains were cloned into pCAMBIA1301 and inoculated into tomato seedlings by agro-inoculation. All plants were grown in insect-proof greenhouses under natural sunlight supplemented with artificial lighting for 14 h a day and a controlled temperature of 25 ± 3°C. The inoculated plants that showed typical symptoms of virus infection at 25 ~ 30 days post inoculation were used for whitefly transmission. Virus infection of all inoculated plants was confirmed by PCR using specific primers (Supplementary Table S1). The disease severity caused by the inoculated TYLCV strains on tomato plants was evaluated visually for 25 days post inoculation. Symptom development was scored using a disease index ranging from 0 to 4, where 0 = no symptoms and 4 = very severe symptoms (severe stunting, leaf curling, cupping, and growth arrest), following the method of Friedmann et al. [26]. Intermediate scores (0.5, 1.5, 2.5, and 3.5) were used to improve the precision of disease severity assessment.

**TYLCV infection of *B. tabaci* and viral titer analysis**

Newly emerged adult whiteflies (2 ~ 4 days post-emergence) were collected in a batch of 50 individuals for an experimental unit and transferred onto tomato leaves infected with either the TYLCV-IL or TYLCV-Mld strain, placed inside large Petri dishes (100 × 40 mm, SPL Life Sciences, Seoul, Korea). After a 24-hour AAP, whiteflies were collected and subjected to RNA and DNA extraction. Each infection treatment was performed with three independent biological replicates.

To determine viral titer dynamics in infected *B. tabaci* over time, adult whiteflies were allowed to feed on TYLCV-infected tomato plants for 24 h to acquire the virus. Then, TYLCV-viruliferous whiteflies were transferred to small Petri dishes (50 × 15 mm; SPL Life Sciences), sealed with a double layer of plastic tape, and provided with 30% sucrose solution for up to

seven days. Each day, a group of 20 insects were collected for DNA extraction and quantitative PCR (qPCR) using specific primers targeting the TYLCV coat protein gene (Supplementary Table S1). Three independent biological replicates were analyzed at each time point, and each biological replicate consisted of 20 pooled adults.

**Test compounds and preparation of commonly used chemicals**

9,10- and 12,13-EpOMEs, and $PGE_2$ were purchased from Cayman Chemical (Ann Arbor, MI, USA). 12-(3-Adamantan-1-ylureido)dodecanoic acid (AUDA), benzyloxycarbonyl-Val-Ala-Asp-fluoromethyl ketone (Z-VAD), arachidonic acid (AA; 5,8,11,14-eicosatetraenoic acid), dexamethasone (DEX; (11β,16α)-9-fluoro-11,17,21-trihydroxy-16-methylpregna-1,4-diene-3-one), esculetin (ESC; 6,7-dihydroxycoumarin), and naproxen (NAP; (S)-(+)-2-(6-methoxy-2-naphthyl) propionic acid) were obtained from Sigma-Aldrich Korea (Seoul, Korea) and dissolved in dimethyl sulfoxide (DMSO) to prepare stock solutions. 5-Bromo-2′-deoxyuridine (BrdU) and anti-BrdU antibody were purchased from Abcam (Cambridge, UK). Terminal deoxynucleotidyl transferase, fluorescein isothiocyanate (FITC)-conjugated anti-rabbit IgG antibody, and 4′,6-diamidino-2-phenylindole (DAPI) were obtained from Thermo Fisher Scientific (Wilmington, DE, USA). Bovine serum albumin (BSA), DMSO, and t-octylphenoxy-polyethoxyethanol (Triton X-100) were purchased from Sigma-Aldrich Korea. Phosphate-buffered saline (PBS) was prepared with 100 mM phosphoric acid containing 0.7% NaCl and adjusted to pH 7.4 with 1 M NaOH.

The compounds were selected based on their established use in insect oxylipin studies [16-19] as functional modulators of eicosanoid or epoxy-fatty-acid signaling pathways, and the tested concentrations were chosen within ranges commonly used for insect physiological assays.

**RNA interference (RNAi) treatment to *B. tabaci* using double-stranded RNA (dsRNA)**

Template DNAs were amplified by PCR using gene-specific primers (Supplementary Table S1) containing the T7 promoter sequence at their 5′ ends, following previously described methods [25]. The resulting PCR products were used as templates for *in vitro* transcription with the MEGAscript RNAi Kit (Ambion, Austin, TX, USA) according to the manufacturer's instructions. The synthesized dsRNAs were combined with Metafectene PRO (Biontex, Munchen, Germany) at a 1:1 (v/v) ratio and incubated at room temperature (RT) for 30 min to form dsRNA–liposome complexes. Oral delivery of dsRNA was performed using a parafilm-based feeding apparatus prepared in sterile small Petri dishes. A synthetic diet containing 30% (w/v) sucrose and dsRNA at a final concentration of 500 ng/μL was applied to the inner surface of a stretched parafilm membrane. The membrane was lightly punctured at the feeding zone to enable stylet access. Adult *B. tabaci* (20 individuals per replicate) were placed on the outer side of the membrane and maintained under controlled conditions (25 ± 1°C, 70 ± 5% relative humidity, 14:10 h light:dark cycle) to allow ingestion of the dsRNA-containing diet. Gene silencing efficiency was evaluated by quantitative PCR within 48 h following exposure.

**Test compound treatment to *B. tabaci***

To treat the test compounds including AA (1 μg/mL), 12,13-EpOME (0.1 μg/mL), Z-VAD-FMK (50 μM), AUDA (10 μg/mL), DEX (1 μg/mL), NAP (1 μg/mL), ESC (1 μg/mL), $PGE_2$ (0.1 μg/mL), $PGD_2$ (0.1 μg/mL), and $PGF_{2\alpha}$ (0.1 μg/mL) to the adult whiteflies, 1 g of TYLCV-infected tomato leaves were homogenized with 10 mL of filter (0.22 μm pore size)-sterilized PBS (1:10, w/v) and centrifuged at 14,000× *g* for 5 min. The supernatant was used as the virus suspension and mixed with 30% (w/v) sucrose solution at a 1:1 ratio. Next, each compound

was mixed with this mixture (to get the final concentration as mentioned before) and placed on the double layers of parafilm that covered the opening of the small Petri dish as explained above. Treatments were conducted in triplicate with 20 adults per replicate, and after a 24-h feeding period, insects were harvested for DNA or RNA extraction to determine viral titers and mRNA levels, respectively.

**Nucleic acid extraction, qPCR, and RT-qPCR**

For transcript analysis, total RNA was isolated from the treated whiteflies using TRIzol reagent (Ambion) according to the manufacturer's instructions. The concentration and purity of RNA samples were assessed using a NanoDrop spectrophotometer (Thermo Fisher Scientific). Reverse transcription was performed with 100 ng of total RNA using the RT-Premix kit (Intron Biotechnology, Seoul, Korea) containing an oligo(dT) primer, following the manufacturer's protocol.

To quantify the viral titer, the treated whiteflies were homogenized in DNA extraction buffer (Biosearch Technologies, Seoul, Korea). The homogenate was incubated at 100°C for 5 min to lyse the cells, followed by centrifugation at 14,000× *g* for 3 min. The resulting supernatant was transferred to new tubes and used as the DNA template for subsequent experiments.

Gene expression levels and viral titers were determined by RT-qPCR and qPCR, respectively, using a Step One Plus Real-Time PCR System (Applied Biosystems, Singapore) and Power SYBR Green PCR Master Mix (Toyobo, Osaka, Japan) according to the manufacturer's instructions. Each RT-qPCR reaction (20 μL total volume) contained 10 μL of 2× Power SYBR Green PCR Mix, 100 ng of DNA or cDNA template, and 10 pmol of each specific primer (Supplementary Table S1). The *Bt-EFα* (Supplementary Table S1) gene was

used as an internal reference for normalization. Amplification specificity was confirmed by melting curve analysis. Each qPCR reaction was performed in triplicate as technical replicates, and each treatment included three independent biological replicates. Relative gene expression levels were calculated using the comparative Ct ($2^{-\Delta\Delta Ct}$) method [27].

**Insect sample preparation to quantify EpOMEs**

To determine EpOME levels in *B. tabaci* following TYLCV infection, lipids were extracted from both non-viruliferous and viruliferous adult whiteflies. After a 24-hour AAP on TYLCV-infected tomato plants, 200 adult whiteflies were collected and washed three times with chilled PBS. Each sample was subjected to three rounds of ultrasonic homogenization (1 min each) in PBS using an ultrasonicator (Bandelin Sonoplus, Berlin, Germany) set to 80% power. The pH of the homogenate was adjusted to 4.0 with 1 N HCl. Lipids were extracted by adding 1 mL of ethyl acetate, and the upper organic phase was separated. The remaining aqueous phase was re-extracted twice with ethyl acetate. Combined extracts were evaporated under a gentle nitrogen stream to a final volume of approximately 500 µL and loaded onto a small silicic acid column (2 × 90 mm; containing 30 mg of Type 60A silicic acid, 100–200 mesh; Sigma-Aldrich Korea). Sequential elusion was performed with solvents of increasing polarity in the order of 100% ethyl acetate, ethyl acetate/acetonitrile (1:1, v/v), acetonitrile/methanol (1:1, v/v), and finally 100% methanol. The ethyl acetate fraction was collected and used for EpOME quantification. Each treatment was performed with three independent biological replicates, and each biological replicate consisted of 200 independently collected adult whiteflies.

**LC-MS/MS analyses**

EpOME quantification was performed using an LC–MS/MS system (QTrap 4500; AB Sciex,

Framingham, MA, USA) equipped with an autosampler, binary pump, and column oven. Chromatographic separation was achieved on a C18 column (2.1 × 150 mm, 2.7 μm; Osaka Soda, Osaka, Japan) maintained at 40°C. The mobile phases consisted of 0.1% formic acid in water (solvent A) and 0.1% formic acid in acetonitrile (solvent B). The gradient program was as follows: 30% B (0–2 min), 30–65% B (2–12 min), 65–95% B (12–12.5 min), 95% B (12.5–25 min), and re-equilibration at 30% B (25–30 min). The flow rate was set to 0.4 mL $min^{-1}$, the injection volume was 10 μL, and the autosampler temperature was maintained at 5°C. Detection was performed using an electrospray ionization (ESI) source in negative ion mode. Optimized ion source parameters were as follows: temperature, 600°C; curtain gas, 32 L $min^{-1}$; ion gas, 60 L $min^{-1}$; and spray voltage, –4,000 V. Data were acquired in multiple reaction monitoring mode using nitrogen as the collision gas. Peak detection, integration, and quantification were conducted with MassView 1.1 software (AB Sciex). Each independently prepared biological replicate was analyzed once by LC–MS/MS, and no separate technical injection replicates were performed.

**KEGG analysis of *B. tabaci* between viruliferous and nonviruliferous adults**

RNA-seq data from non-viruliferous (BioSample: SAMN10060942; SRA: SRS3774498) and TYLCV-viruliferous *B. tabaci* MED after 24 h of feeding (BioSample: SAMN10060936; SRA: SRS3774502) were retrieved from the NCBI database. Raw reads were processed and analyzed using CLC Genomics Workbench (v24.0.1; QIAGEN, Hilden, Germany). Low-quality reads and adapter sequences were removed using the Trim Reads tool prior to mapping against the *B. tabaci* reference genome (GenBank accession no. GCF_918797505.1). Gene expression levels were quantified and normalized as transcripts per million (TPM) to enable comparisons between non-viruliferous and TYLCV-infected samples. Gene identifiers were assigned based

on annotated gene symbols and corresponding LOC numbers obtained from the *B. tabaci* general feature format file. Differentially expressed genes (DEGs) between non-viruliferous and viruliferous groups were identified using the Differential Expression for RNA-Seq tool in CLC Genomics Workbench. Functional annotation was performed using Kyoto Encyclopedia of Genes and Genomes (KEGG) pathway analysis. Gene symbols were converted to KEGG gene IDs using the bioDBnet ID conversion tool, and pathway mapping was conducted with KofamKOALA (KEGG; https://www.genome.jp/tools/kofamkoala). KEGG pathway enrichment analysis was used to identify metabolic and functional pathways significantly affected by TYLCV infection based on differential TPM profiles. Data visualization was performed using R software (version 4.3.1) with the ggplot2 package.

**Bioinformatics to predict eicosanoid- and EpOME-associated genes from *B. tabaci* genome**

To predict *$PLA_2$*, *CYP*, and *sEH* genes of *B. tabaci*, all annotated amino acid sequences of these gene families were retrieved from the NCBI-GenBank database (www.ncbi.nlm.nih.gov) and aligned with their orthologs from other representative insects and vertebrate species (Supplementary Table S2). Similarly, to identify eicosanoid-associated genes, annotated amino acid sequences were obtained from the *B. tabaci* genome and compared with known orthologs from other insects and vertebrates (Supplementary Table S2). Candidate Bt-PGES2 and Bt-$PGE_2$R were identified based on sequence homology and phylogenetic clustering with reported insect and vertebrate PGES2 (microsomal PGES-2) and $PGE_2$ receptor proteins, respectively. Their annotation was therefore assigned according to orthologous relationships and conserved domain architecture revealed by comparative bioinformatic analyses. Multiple sequence alignments were conducted using ClustalW within MEGA11 [28]. Their phylogenetic trees

were constructed using the Neighbor-joining method, with 1,000 replicates to calculate bootstrap values, employing MEGA11.

**Fluorescence *in situ* hybridization (FISH) analysis**

After 24 h-feeding on the TYLCV-infected diet, adult whitefly midguts were dissected on sterilized glass slides and fixed with 4% paraformaldehyde for 1 h at RT. Following fixation, the tissues were rinsed with 1× PBS and permeabilized with 1% Triton X-100 in PBS for 1 h at RT. After an additional PBS wash, the samples were rinsed in 2× saline-sodium citrate (SSC) buffer and incubated at 42°C with 25 μL of pre-hybridization buffer containing 2 μL of yeast tRNA, 2 μL of 20× SSC, 4 μL of dextran sulfate, 2.5 μL of 10% SDS, and 14.5 μL of deionized $H_2O$. The incubation was carried out for 1 h under dark and humid conditions. The pre-hybridization buffer was then replaced with a hybridization buffer consisting of 5 μL of deionized formamide and 1 μL of fluorescein-labeled oligonucleotide probe in 19 μL of the initial pre-hybridization mix. DNA oligonucleotide probes targeting the TYLCV *cp* gene (Supplementary Table S1) were labeled at the 5′ end with fluorescein amidite (FAM) and purified by high-performance liquid chromatography (Bioneer, Daejeon, Korea). Slides were covered with RNase-free coverslips and incubated overnight (18 h) in a humid chamber at 42°C. Following hybridization, the gut tissues were washed twice with 4× SSC for 10 min each, followed by a 5 min wash in 4× SSC containing 1% Triton X-100 at RT. The samples were then washed three times with 4× SSC, incubated at 37°C for 30 min in 1% anti-rabbit FITC-conjugated antibody (Thermo Fisher Scientific) in PBS, and protected from light. After two washes with 4× SSC (10 min each) and one wash with 3× SSC, the midgut samples were air-dried. A drop of 50% glycerol was added, and after a 15 min incubation at RT, the samples were mounted with a coverslip and examined under a fluorescence microscope (DM2500,

Leica, Wetzlar, Germany) at 200× magnification. Each experimental treatment was performed in triplicate using different individual insects, and a midgut from each insect was examined per biological replicate.

**Immunofluorescence assay**

Twenty-four hours after TYLCV infection or TYLCV infection combined with compound treatment, adult whitefly midguts were dissected on sterilized glass slides and fixed in 4% formaldehyde for 1 h at RT. After washing three times with PBS, the midguts were permeabilized with 1% Triton X-100 in PBS for 1 h at RT. Following three additional washes with PBS, the samples were blocked with 10% BSA in PBS for 30 min at RT. The midguts were then incubated for 2 h at RT in a humid chamber with either a TYLCV coat protein-specific antibody (#NAV1034-001S, PhytoAB Inc., San Francisco, CA, USA) or an antibody against cleaved caspase-3 (Asp175) (#9661, Cell Signaling Technology, Boston, MA, USA). After careful washing with PBS, the samples were incubated with 1% FITC-conjugated anti-rabbit secondary antibody (Thermo Fisher Scientific, Seoul, Korea) in PBS for 2 h at RT. Following three washes with PBS, the samples were mounted in 50% glycerol, covered with a coverslip (18 × 18 mm; Marienfeld, Königshofen, Germany), and observed under a fluorescence microscope (DM2500; Leica, Wetzlar, Germany) at 200× magnification. Each treatment was conducted with three biological replicates using different individual insects, and a midgut from each insect was examined per replicate.

**Terminal deoxynucleotidyl transferase dUTP nick end labeling (TUNEL) assay**

TUNEL assays were performed using the *in-situ* Cell Death Detection kit (Abcam, Cambridge, UK). Adult whitefly midguts were dissected in PBS and placed on 22 × 22 mm coverslips. The

tissues were then incubated with 10 μM BrdU and terminal transferase for 1.5 h. Following incubation, samples were fixed in 4% paraformaldehyde for 1 h at RT, rinsed with PBS, and permeabilized with 0.3% Triton X-100 in PBS for 2 h. After permeabilization, tissues were blocked for 1 h with 5% BSA in PBS and subsequently incubated with an anti-BrdU antibody (1:15 dilution in blocking buffer) for 1 h at RT. Unbound antibodies were removed by three PBS washes, followed by incubation with an FITC-conjugated anti-mouse IgG secondary antibody (1:300 dilution in blocking buffer) for 1 h. After three additional PBS washes, 10 μL of DAPI solution (1:1,000 dilution in blocking buffer) was added and incubated for 5 min at RT. Samples were rinsed with PBS, mounted with 10 μL of a glycerol–PBS mixture, and covered with a glass coverslip. Fluorescence signals were observed using a Leica DFC450C fluorescence microscope in FITC mode. Each experimental treatment was performed in triplicate, and one midgut was examined per biological replicate.

### Statistical analysis

All statistical analyses were performed using SAS software with the PROC GLM procedure. For all experiments, statistical analyses were conducted using biological replicates, and technical replicates, when performed, were averaged before analysis. The mean value of each biological replicate was used as a single unit for statistical testing. Differences among more than two groups were analyzed by one-way ANOVA followed by the least significant difference (LSD) test at $\alpha = 0.05$. For comparisons between two groups, Student's t-test was used when appropriate. Data are presented as mean ± SD.

## Results

### Fatty acid metabolism is altered in whiteflies infected with TYLCV

To examine the early dynamics of TYLCV infection in the vector intestine, viral localization was analyzed using fluorescence *in situ* hybridization (FISH) at different time points after virus acquisition (Fig. 1A). TYLCV signals were first detected as early as 6 h post-infection, mainly in the midgut (MG) and hindgut (HG) as weak fluorescence signals and appeared as small discrete foci, indicating the initial entry of virions into intestinal tissues. The signals became more apparent at 12 h and increased further at 24 h, indicating progressive viral accumulation in the intestinal tissues. By 48 h post-infection, TYLCV signals were stronger and more widely distributed in the midgut and hindgut, reflecting further accumulation of TYLCV in the vector gut. In contrast, no viral signal was detected in the foregut, which appeared as a thin thread-like structure (Supplementary Figure S1). Moreover, non-viruliferous control insects showed no detectable TYLCV signal, confirming the specificity of the FISH detection. These results indicate a time-dependent increase of TYLCV accumulation in the intestine of *B. tabaci*.

Transcriptomic analysis (Supplementary Table S3) of the infected adults revealed that TYLCV infection altered the gene expression associated with major nutrients and their energy metabolism (Fig. 1B). KEGG pathway analysis on the transcriptome of *B. tabaci* adults after a 24-h acquisition access period (AAP) showed that one of the most noticeable changes after the viral infection was observed in fatty acid metabolism, in which its synthesis was active in nonviruliferous but not in viruliferous insects, while its modification was active in viruliferous but not in nonviruliferous insects, suggesting potential alterations in fatty acid metabolism associated with TYLCV infection. It is worth noting that the RNA-seq analysis, based on publicly available datasets, provided preliminary insights into potential alterations in metabolic pathways associated with TYLCV infection.

**Two oxylipins oppositely regulate TYLCV titers in whiteflies**

Two types of oxylipins, $PGE_2$ and EpOMEs, which have been known to be functional in insects [15], are derived from phospholipids through oxygenation pathways (Fig. 2A). The effects of these oxylipins on TYLCV titers were examined in whiteflies. The precursors, arachidonic acid (AA) and linoleic acid (LA), exhibited opposite effects on viral accumulation, with AA significantly reducing and LA increasing viral accumulation (Fig. 2B). The viral titers modulated by AA and LA treatments were quantified by qPCR (Fig. 2C) and immunofluorescence assay (IFA) (Fig. 2D). Among eicosanoids resulting from AA, three PGs were compared for their antiviral activities against TYLCV because they were detected in other insects [15], $PGE_2$ showed the strongest suppression of viral titers, whereas $PGF_{2\alpha}$ had no detectable effect (Fig. 2E). Therefore, $PGE_2$ was selected for subsequent analyses, as it exhibited the strongest antiviral activity among the prostaglandins tested. In contrast, both EpOME isomers significantly enhanced TYLCV titers, with 12,13-EpOME showing a stronger effect than 9,10-EpOME (Fig. 2F). Together, these results indicate contrasting effects of eicosanoids and EpOMEs on TYLCV accumulation, with $PGE_2$ reducing viral titers and EpOME isomers increasing them.

**Up-regulation of $PGE_2$ signaling components in TYLCV-infected whiteflies**

$PGE_2$ biosynthesis is initiated by the catalytic activity of $PLA_2$, which releases AA from membrane phospholipids (Fig. 3A). Pharmacological inhibition of $PLA_2$ using dexamethasone (DEX) resulted in a significant increase in TYLCV titers in the whiteflies. Similarly, inhibition of cyclooxygenase (COX) or lipoxygenase (LOX) also increased the viral titers, with naproxen (NAP) treatment specific to COX being more potent than esculetin (ESC) treatment specific to LOX.

Four *$PLA_2$* genes were predicted from the *B. tabaci* genome and classified through a

phylogenetic analysis into distinct $PLA_2$ groups: *$BtPLA_2$-A* (*$iPLA_2$*, Group VI), *$BtPLA_2$-B* (*$LpPLA_2$*, Group VIII), *$BtPLA_2$-C* (*$sPLA_2$*, Group III), and *$BtPLA_2$-D* (*$LPLA_2$*, Group XV) (Fig. 3B). All four genes were expressed across developmental stages from egg to adult (Fig. 3C). Upon TYLCV infection, *$BtPLA_2$-A* and *$BtPLA_2$-C* were significantly up-regulated, whereas the other two genes showed no significant changes (Fig. 3D). RNAi-mediated silencing of *$BtPLA_2$-A* or *$BtPLA_2$-C* increased the viral titers, while knockdown treatments of the other two *$PLA_2$* genes did not change the viral titers (Fig. 3E).

$PGE_2$ synthase (*PGES2*) catalyzes the conversion of $PGH_2$ to $PGE_2$ following AA oxygenation by COX (Fig. 4A). $PGE_2$ exerts its effects through binding to the $PGE_2$ receptor (*$PGE_2R$*). *Bt-PGES2* was identified as a candidate *PGES2* ortholog from the annotated *B. tabaci* genome by sequence homology and phylogenetic analysis with known insect and vertebrate PGES2/mPGES2 proteins. *Bt-$PGE_2R$* was predicted in the same manner, and both genes clustered with hemipteran orthologs, distinct from other insect groups (Fig. 4B). These genes were expressed throughout all developmental stages (Fig. 4C) and significantly up-regulated following TYLCV infection (Fig. 4D). RNAi treatment specific to either *Bt-PGES2* or *Bt-$PGE_2R$* significantly increased the viral titers in viruliferous whiteflies (Fig. 4E). Together, these results indicate that TYLCV infection upregulated genes associated with the eicosanoid signaling pathway, including those linked to $PGE_2$ signaling in *B. tabaci*.

**Up-regulation of EpOME biosynthesis in TYLCV-infected whiteflies**

Two EpOME isomers were detected in *B. tabaci* using LC-MS/MS analysis (Fig. 5A). Their concentrations increased more than two-fold following TYLCV infection. Inhibition of EpOME degradation to DiHOME using AUDA significantly increased viral titers in viruliferous whiteflies (Fig. 5B). AUDA treatment functionally supports the involvement of

EpOME degradation-associated activity in TYLCV accumulation, although EpOME stabilization after AUDA treatment was not directly quantified in *B. tabaci*. In addition, supplementation with an EpOME analog (AS56) [19] significantly enhanced viral accumulation. These results suggest the involvement of candidate genes associated with EpOME biosynthesis and degradation in *B. tabaci* and their potential association with TYLCV accumulation.

To identify EpOME-biosynthetic enzymes, cytochrome P450 (*CYP*) homologs known for their EpOME-biosynthetic function were phylogenetically analyzed (Fig. 6A). Three *CYP* genes (*Bt-CYP5*, *Bt-CYP6*, and *Bt-CYP7*) clustered with known EpOME synthases and were expressed across all developmental stages (Fig. 6B). Among them, only *Bt-CYP6* was significantly up-regulated following TYLCV infection (Fig. 6C). RNAi knockdown experiments demonstrated that silencing *Bt-CYP6* significantly reduced viral titers, whereas knockdown treatments of the other *CYP* genes had no effect (Fig. 6D), supporting the involvement of *Bt-CYP6* in EpOME-associated metabolism during viral infection.

Candidate EpOME-degrading enzymes were predicted by phylogenetic analysis using a dataset that included validated or annotated insect *sEH* and juvenile hormone epoxide hydrolase (*JHEH*) genes, together with representative vertebrate epoxide hydrolases. The reference sequences were obtained from *F. occidentalis*, *Spodoptera exigua*, *Anopheles gambiae*, *Aedes aegypti*, *Bombyx mori*, *Apis mellifera*, *Homo sapiens*, *Mus musculus*, and *Rattus norvegicus* among others. The analysis identified four epoxide hydrolase genes: one membrane-bound *JHEH* and three soluble forms (*sEH1–sEH3*) (Fig. 7A). All genes were expressed across developmental stages (Fig. 7B). Upon TYLCV infection, expression of *Bt-sEH1* ~ *Bt-sEH3* was significantly suppressed, whereas *Bt-JHEH* expression remained unchanged (Fig. 7C). RNAi-mediated silencing of *Bt-sEH2* or *Bt-sEH3* significantly increased

viral titers, while knockdown of *Bt-sEH1* or *Bt-JHEH* had no effect (Fig. 7D), indicating that *Bt-sEH2* and *Bt-sEH3* may contribute to EpOME turnover during TYLCV infection.

These results indicate the EpOME-associated metabolic genes of *B. tabaci*, in which *Bt-CYP6* is associated with EpOME biosynthesis and *Bt-sEH2*/*sEH3* are associated with EpOME degradation.

**Sequential expression profile of eicosanoid and EpOME biosynthesis-associated genes in *B. tabaci* after TYLCV infection**

Two oxylipins ($PGE_2$ and EpOME) exhibited antagonistic activities against regulating TYLCV titers in *B. tabaci*. To examine their temporal production in *B. tabaci* after TYLCV infection, their synthetic genes were monitored in their expressions at different time points post-inoculation (Fig. 8). Three genes (*$BtPLA_2$-A*, *$BtPLA_2$-C*, and *Bt-PGES2*) associated with $PGE_2$ biosynthesis were up-regulated immediately after the viral infection and showed their maximal expression at 1-day post-infection. In contrast, the EpOME biosynthesis gene (*Bt-CYP6*) exhibited relatively later expression patterns, with its maximal expression peaking at 2 ~ 3 days post-infection. Interestingly, the EpOME-degradation genes (*Bt-sEH2*/*sEH3*) were significantly suppressed at 2 ~ 3 days post-infection. These temporal patterns of gene expressions suggest differential regulations of $PGE_2$ and EpOME biosynthesis during viral infection in *B. tabaci*.

**Validation of EpOME as a proviral signal using two TYLCV strains**

To support the role of EpOME as a proviral factor for TYLCV, two viral strains with different virulence were tested for their ability to induce EpOME levels in *B. tabaci*. Two TYLCV strains, TYLCV-Mld and TYLCV-IL, were transmitted to the same tomato cultivar using a single

whitefly cohort (Fig. 9A). Thirty days post-inoculation, both strains induced typical disease symptoms, with TYLCV-IL causing significantly more severe symptoms than TYLCV-Mld. Viral titers in the intestines of viruliferous whiteflies were significantly ($F = 168.16$; df = 1, 32; $P < 0.0001$) higher in TYLCV-IL-infected individuals compared to TYLCV-Mld, as determined by immunofluorescence and qPCR analyses (Fig. 9B). This difference was evident as early as 2 days post-infection, coinciding with significantly higher *Bt-CYP6* expression in TYLCV-IL-infected whiteflies (Fig. 9C). In contrast, expression of *Bt-sEH2* and *Bt-sEH3* was more strongly suppressed in TYLCV-IL-infected whiteflies than in those infected with TYLCV-Mld.

**Apoptosis in the intestine of *B. tabaci* as a proviral response to TYLCV infection**

TYLCV infection induced apoptosis in the intestine of TYLCV-IL-infected *B. tabaci*, particularly in the midgut including caeca, as detected by TUNEL assays (Fig. 10A). Apoptotic signals were reduced by $PGE_2$ supplementation but enhanced by 12,13-EpOME treatment in viruliferous whiteflies. Expression levels of two apoptosis-associated caspases, the initiator caspase *Dronc* and the effector caspase-1 (*Cas1*), were significantly upregulated following TYLCV infection (Fig. 10B), with higher induction observed in TYLCV-IL-infected whiteflies compared to TYLCV-Mld. The apoptosis was further supported by IFA specific to cleaved caspase-3 acting as an apoptosis executor (Fig. 10C). TYLCV induced the positive IFA signal in the midgut, in which higher induction was observed in TYLCV-IL-infected whiteflies compared to TYLCV-Mld. The addition of EpOME enhanced the apoptotic signal while that of $PGE_2$ suppressed the signal intensity. Functional involvement of apoptosis in viral accumulation was further supported by treatment with the apoptosis inhibitor Z-VAD, which significantly reduced viral titers in whiteflies infected with either strain (Fig. 10D).

514

515 **Immune-associated genes of *B. tabaci* function as either proviral or antiviral factors**
516 **during TYLCV infection**

517 Six immune-associated genes that were upregulated following TYLCV infection were selected
518 for functional analysis (Fig. 11). EpOME treatment induced the expressions of *defensin*,
519 *cathepsin-B*, and *cathepsin-L*, while it suppressed the expressions of *knottin*, *PGRP*, and
520 *cathepsin-F* (Fig. 11A). Conversely, $PGE_2$ treatment showed expression patterns opposite to
521 those induced by EpOME, consistent with their antagonistic roles in regulating TYLCV
522 infection. To clarify this expression control, individual RNAi treatments specific to each of the
523 immune genes were performed and evaluated for the control of the viral titers (Fig. 11B,
524 Supplementary Figure S2). RNAi-mediated suppression of *defensin*, *cathepsin-B*, or *cathepsin-*
525 *L* significantly reduced viral titers in viruliferous whiteflies, indicating proviral roles. In
526 contrast, knockdown treatments of *knottin*, *PGRP*, or *cathepsin F* significantly increased viral
527 titers, suggesting antiviral functions.

528

529 **A viral factor, C2, modulates host vector in up-regulating EpOME level upon TYLCV**
530 **infection**

531 To identify the virulence factor derived from TYLCV responsible for the up-regulation of host
532 EpOME levels, six viral genes (V1, V2, C1, C2, C3, and C4; Fig. 12A) encoded in the TYLCV
533 genome were functionally evaluated using an RNAi-based loss-of-function approach. Adult
534 whiteflies infected with TYLCV were individually treated with gene-specific dsRNAs
535 ($dsRNA^{V1}$, $dsRNA^{V2}$, $dsRNA^{C1}$, $dsRNA^{C2}$, $dsRNA^{C3}$, and $dsRNA^{C4}$). All RNAi treatments
536 efficiently suppressed their corresponding target genes for at least 48 h post-infection
537 (Supplementary Figure S3). Under these knockdown conditions, the expression levels of the

EpOME biosynthetic gene (*Bt-CYP6*) and the EpOME degradation genes (*Bt-sEH2* and *Bt-sEH3*) were quantified (Fig. 12B). Among all viral genes tested, silencing of *TYLCV-C2* alone disrupted EpOME pathway regulation. Specifically, RNAi specific to *TYLCV-C2* markedly suppressed the TYLCV-induced up-regulation of *Bt-CYP6*, whereas knockdown of other viral genes had no significant effect. In addition, *TYLCV-C2* silencing prevented the virus-associated down-regulation of *Bt-sEH2* and *Bt-sEH3* expression, in contrast to the other RNAi treatments. For control, $dsRNA^{C2}$ did not change expressions of *Bt-CYP6*, *Bt-sEH2*, and *Bt-sEH3* in the non-viruliferous whiteflies (Supplementary Figure S4). These results indicate that TYLCV-C2 appears to be a major viral factor associated with EpOME pathway modulation by simultaneously enhancing EpOME biosynthesis and suppressing EpOME degradation in TYLCV-infected whiteflies. To further validate the role of TYLCV-C2-mediated EpOME signaling in viral infection, a rescue experiment was performed by orally supplying 12,13-EpOME to the TYLCV-C2-silenced viruliferous whiteflies. Exogenous 12,13-EpOME effectively restored viral accumulation to levels comparable to the dsCON control (Fig. 12C), supporting the role of TYLCV-C2 in host-mediated EpOME up-regulation to facilitate viral infection.

## Discussion

It has been recognized that TYLCV is not a passive passenger within its vector but actively reshapes whitefly development, immunity, and behavior to optimize its own transmission [29]. TYLCV infection alters whitefly life-history traits, feeding behavior, and stress tolerance, illustrating a multifaceted strategy of vector manipulation. Despite these advances, the molecular mechanisms linking viral sensing in the gut to a durable, system-wide permissive state within the vector have remained poorly defined. Here, we demonstrate that TYLCV

562 achieves this permissive state by rewiring vector oxylipin signaling, shifting the balance from
563 antiviral eicosanoids toward proviral EpOMEs. In addition, this study identifies the viral factor
564 responsible for this endocrine signal change.

565 This study demonstrated a progressive infection of TYLCV in the host intestine.
566 Initially, the infection was observed in the midgut and hindgut, but not in the foregut. Later, the
567 infection foci increased in number. Furthermore, the viral titers increased in a whole-body
568 sample as well as in the intestine, supporting viral accumulation of TYLCV in the vector insect.
569 Although TYLCV was previously classified as a circulative, non-propagative virus transmitted
570 by the whitefly *B. tabaci*, accumulating evidence indicates that TYLCV can replicate within
571 its vector in a circulative–propagative transmission mode [30, 31]. During this viral
572 multiplication, TYLCV must have overcome defensive barriers derived from the whiteflies.
573 Successful circulative transmission of TYLCV requires that the virus traverse multiple
574 anatomical and physiological barriers while preserving vector viability [29, 32]. At least three
575 major anatomical barriers of the whiteflies restrict TYLCV movement: the midgut epithelial
576 cells for entry and exit, the hemocoel, and the salivary gland cells for entry and exit [33]. Viral
577 entry into the midgut epithelium is mediated by the CUBAM receptor complex, composed of
578 cubilin and amnionless, and proceeds through clathrin-dependent endocytosis [34]. Following
579 receptor binding, TYLCV is internalized into endosomal compartments, where low pH
580 promotes virion dissociation from the receptor. Subsequent trafficking decisions determine
581 whether virions are degraded in lysosomal compartments or transported across the basal
582 membrane, a process involving sorting nexins such as Snx12 [33, 34]. The resulting free virions
583 in the midgut epithelial cells may transform host cells into favorable conditions for viral
584 replication.

585 One of the physiological changes after viral infection was apoptosis in the midgut

586 epithelium of the viruliferous *B. tabaci*. This phenomenon has also been reported in previous
587 studies showing that TYLCV activates apoptotic pathways in *B. tabaci* and that experimental
588 manipulation of apoptosis can alter viral accumulation, supporting a functional link between
589 apoptosis and transmission biology [35, 36]. Our findings extend this framework by
590 demonstrating that intestinal apoptosis intensity is positively correlated with viral titer. This
591 positive relation between apoptosis and TYLCV titer was further supported by treatment with
592 the apoptosis inhibitor, Z-VAD, which led to a reduction in the viral titer. Furthermore, this
593 study demonstrated that apoptosis in the gut is enhanced by EpOME signaling while being
594 suppressed by eicosanoid signaling. The effect of EpOME treatment on gut apoptosis was
595 further supported by the induction of caspase genes associated with the initiation and execution
596 of apoptosis. Although apoptosis is classically antiviral in many insect–virus systems,
597 including other plant viruses such as tomato spotted wilt virus [23], controlled epithelial
598 turnover or barrier remodeling may facilitate virion movement across the gut wall or reduce
599 intracellular degradation routes that would otherwise destroy virions. This interpretation is
600 consistent with models in which endo-lysosomal processing represents a critical checkpoint
601 determining viral degradation versus successful transcytosis [33]. Recent studies of
602 begomovirus–whitefly interactions emphasize that immune pathways such as apoptosis,
603 autophagy, Toll, and JAK/STAT function as checkpoints that viruses must negotiate to establish
604 persistent infections and maintain transmissibility [37]. In parallel, detailed mechanistic studies
605 have elucidated how TYLCV crosses the midgut barrier through receptor-mediated endocytosis
606 and intracellular trafficking routes that balance transcytosis against degradation [33, 34]. While
607 these studies define where and how TYLCV moves within the vector, they do not fully explain
608 how the internal immune-metabolic environment becomes permissive over time. Our results
609 add a complementary layer by showing that TYLCV infection is associated with alterations in

lipid mediator signaling, thereby influencing multiple immune and physiological checkpoints simultaneously. Specifically, we demonstrate that eicosanoid signaling suppresses TYLCV accumulation, whereas EpOMEs enhance viral titers. Indeed, TYLCV infection transcriptionally favors EpOME accumulation by inducing the EpOME synthase *Bt-CYP6* while suppressing EpOME-degrading sEH (*Bt-sEH2* and *Bt-sEH3*). Moreover, exogenous EpOME supplementation restores viral accumulation. Together, these results position oxylipin remodeling as an upstream coordinator of TYLCV-mediated vector manipulation. It was notable that remarkable changes in fatty acid metabolism were observed in DEG analysis between nonviruliferous and viruliferous whiteflies. This supports enhanced oxylipin production in response to TYLCV infection. EpOMEs and their corresponding DiHOMEs are well characterized in mammals as cytochrome P450–derived linoleate epoxides with immunomodulatory properties [38]. In insects, EpOME biology has only recently begun to emerge. EpOMEs have been reported as immune suppressors in lepidopteran insects, and inhibition of soluble epoxide hydrolase can stabilize epoxy-fatty acids and mimic immunosuppressive phenotypes [16]. Insect epoxide hydrolases are evolutionary diverse enzymes with functions extending beyond juvenile hormone metabolism to regulation of endogenous lipid mediators [39]. Our study advances this literature by demonstrating EpOME-mediated immune regulation in a hemipteran vector and by linking EpOME accumulation with increased viral accumulation and transmission-related phenotypes.

EpOME signaling may act upstream of selected immune-associated effectors, selectively reshaping immune architecture rather than globally suppressing immunity. PGRPs function as upstream immune sensors and act as pattern-recognition receptors in insects and are implicated in antiviral defense signaling [40, 41]. In our study, PGRP acted as an antiviral factor and was suppressed by EpOME signaling, suggesting that TYLCV may dampen selected

immune-sensing components without disabling immune competence. Cathepsins displayed similar functional specialization: cathepsin-B and -L acted as proviral factors and were selectively induced by EpOME, whereas cathepsin-F exhibited antiviral activity and was suppressed, consistent with previous reports identifying cathepsin-B as a proviral determinant in *B. tabaci* [42, 43]. Under EpOME-dominant conditions, *defensin* expression increased and was associated with a proviral effect. In contrast, the cysteine-rich knottin peptide showed an antiviral role, its expression being suppressed by EpOME but promoted by eicosanoid signaling. Although defensin is typically considered an antimicrobial peptide involved in host defense [44], our results suggest a context-dependent role in the TYLCV–*B. tabaci* interaction. Similar paradoxical effects have been reported in other host–pathogen systems, where immune effectors support infection tolerance or gut homeostasis, indirectly facilitating persistent pathogen infection [45]. In the whitefly gut, *defensin* induction may help maintain intestinal homeostasis or suppress secondary microbial stress during viral infection, thereby creating conditions that favor stable TYLCV persistence and transmission. In *Nilaparvata lugens*, defensin plays a crucial role in maintaining a symbiotic bacterium, *Burkholderia capacia*, under nicotine-induced stress [46]. Importantly, knottin-1 has been previously shown to function as a critical antiviral restriction factor in *B. tabaci*, limiting TYLCV acquisition and transmission [47]. Functional divergence among AMP classes has been reported in other insect–pathogen systems, where distinct AMPs contribute differently to resistance versus tolerance strategies [14, 48]. Our findings extend this concept to TYLCV transmission. Taken together, our results indicate that TYLCV infection is associated with transcriptional regulation of genes linked to eicosanoid and EpOME signaling pathways, which functionally correlate with viral accumulation in the vector. These findings suggest that oxylipin signaling modulates host cellular physiological responses, including immune gene expression and apoptosis in the

whitefly gut, thereby influencing TYLCV accumulation rather than directly targeting the nuclear viral replication machinery.

Among viral genes, *TYLCV-C2* was identified as a viral determinant responsible for up-regulating EpOME signaling in the viruliferous *B. tabaci*. To test this hypothesis, we used individual RNAi specific to each viral gene of TYLCV. To the best of our knowledge, this study is the first experimental demonstration of the viral gene expressions in insect host and their suppression by RNAi in TYLCV-*B. tabaci* system. TYLCV-C2 promotes EpOME accumulation by inducing *Bt-CYP6* and suppressing *Bt-sEH2/3*, and the reduced viral accumulation in the TYLCV-C2 knockdown background could be rescued by exogenous EpOME application. TYLCV-C2 is a multifunctional virulence protein that subverts host ubiquitination pathway, suppress plant defenses and manipulate hormone-associated signaling, including jasmonic acid and salicylic acid pathways, to favor viral infection and vector performance [49, 50]. A recent study further demonstrated that TYLCV-C2 alters salicylic acid–linked defense signaling in plants in ways that facilitate whitefly transmission [51]. Our findings broaden the viral factor framework by showing that, in addition to its roles in the plant host, TYLCV-C2 contributes to changes in the vector's immune-metabolic environment.

Differences among TYLCV strains are often discussed in terms of symptom severity, viral accumulation, and epidemiological spread [5]. However, mechanistic explanations for strain-specific differences in vector competence have largely focused on capsid–receptor interactions or intracellular trafficking efficiency [33, 34]. Comparison of TYLCV-IL and TYLCV-Mld in this study reveals an additional mechanism: the more virulent TYLCV-IL strain induces stronger EpOME pathway activation, higher intestinal viral titers, and more pronounced apoptotic responses. This suggests that strain-specific capacity to reprogram oxylipin signaling contributes to vector competence, a mechanism that can operate in parallel

with entry and trafficking pathways. Notably, our previous work demonstrated that wild-type and resistance-breaking strains of TSWV differentially upregulate EpOME biosynthesis in their thrips vector *F. occidentalis*, supporting a broader role for EpOME signaling in vector–virus interactions [52].

A survival–transmission balance has been proposed in which the JAK/STAT pathway protects whiteflies from TYLCV-associated fitness costs while permitting persistent infection, highlighting that vector immunity is not simply "on" or "off" but is optimized for coexistence with the virus [53]. Our data aligns with this concept and extends it by identifying lipid mediators as rapid, systemic regulators linking metabolic status to immune outcomes. By increasing EpOME levels through C2 activity, TYLCV may shift the vector from an antiviral, eicosanoid-biased state toward a tolerant, EpOME-biased state that supports higher viral loads while preserving vector viability.

## Conclusion

This study advances TYLCV transmission biology by identifying EpOMEs as endocrine-like mediators of vector competence, providing functional genetic evidence for specific EpOME biosynthesis and degradation genes, and supporting TYLCV-C2 as a viral factor involved in vector lipid immune modulation. We propose a working model (Fig. 13) in which TYLCV-C2 contributes to a shift in oxylipin-associated signaling from an eicosanoid-associated antiviral state toward an EpOME-associated proviral state, thereby influencing apoptosis and selected immune-associated effectors in a manner that may favor TYLCV accumulation and transmission.

**List of abbreviations**

AA: Arachidonic acid
AAP: Acquisition access period
AUDA: 12-(3-Adamantan-1-ylureido)dodecanoic acid
BSA: Bovine serum albumin
Cas1: Caspase-1
COI: Cytochrome oxidase I
COX: Cyclooxygenase
CYP: Cytochrome P450 monooxygenase
DEG: Differentially expressed gene
DEX: Dexamethasone
DIC: Differential interference contrast
DiHOME: Dihydroxyoctadecenoic acid
DMSO: Dimethyl sulfoxide
DNA: Deoxyribonucleic acid
Dronc: Death regulator Nedd2-like caspase
dsRNA: Double-stranded RNA
EFα: Elongation factor alpha
ELO: Elongase
EpOME: Epoxyoctadecamonoenoic acid
ESC: Esculetin
ESI: Electrospray ionization
FAM: Fluorescein amidite
FITC: Fluorescein isothiocyanate
FISH: Fluorescence in situ hybridization
HG: Hindgut
IFA: Immunofluorescence assay
IAP: Inhibitor of apoptosis
IR: Intergenic region
JHEH: Juvenile hormone epoxide hydrolase
KEGG: Kyoto Encyclopedia of Genes and Genomes
LA: Linoleic acid
LC–MS/MS: Liquid chromatography–tandem mass spectrometry
LOX: Lipoxygenase
LSD: Least significant difference
MG: Midgut
NAP: Naproxen
PBS: Phosphate-buffered saline
PCR: Polymerase chain reaction
PG: Prostaglandin
$PGD_2$: Prostaglandin $D_2$
$PGE_2$: Prostaglandin $E_2$
$PGE_2R$: Prostaglandin $E_2$ receptor
PGES2: Prostaglandin $E_2$ synthase 2
$PGF_2\alpha$: Prostaglandin $F_2$ alpha
PGRP: Peptidoglycan recognition protein
$PLA_2$: Phospholipase $A_2$
PUFA: Polyunsaturated fatty acid
qPCR: Quantitative polymerase chain reaction
RNA: Ribonucleic acid
RNAi: RNA interference
RT: Room temperature
RT-qPCR: Reverse transcription quantitative polymerase chain reaction
sEH: Soluble epoxide hydrolase
SSC: Saline-sodium citrate

TUNEL: Terminal deoxynucleotidyl transferase dUTP nick end labeling
TYLCV: Tomato yellow leaf curl virus
TYLCV-IL: Tomato yellow leaf curl virus-Israel strain
TYLCV-Mld: Tomato yellow leaf curl virus-Mild strain
Z-VAD: Benzyloxycarbonyl-Val-Ala-Asp-fluoromethyl ketone


## Acknowledgments

The authors thank members of the School of Life Science and Engineering, Gyeongkuk National University, for technical assistance and valuable discussions during this study.


## Author contributions

N.S. and Y.K. conceived and designed the study. N.S., T.-G.S., M.-C.S., J.J., and D.L. performed the experiments and collected the data. N.S. analyzed the data and prepared the figures. E.-J.K. contributed to resources, and scientific discussion. N.S. and Y.K. wrote the original draft of the manuscript. Y.K. supervised the study, acquired funding, and revised the manuscript. All authors reviewed and approved the final manuscript.


## Funding

This work was supported by a grant (No. 2022R1A2B5B03001792) from the National Research Foundation (NRF) funded by the Ministry of Science, ICT and Future Planning, Republic of Korea. It was also supported by the research grant from a Glocal Project of Gyeongkuk National University.


## Data availability

The data supporting this study's findings are available from the corresponding author upon reasonable request.

## Ethics approval and consent to participate

This study did not involve human participants or vertebrate animals. Experiments using *Bemisia tabaci* and tomato plants were conducted under institutional biosafety and research guidelines; no specific ethical approval was required.

## Consent for publication

Not applicable.

## Competing interests

The authors declare no competing interests.

## References


1. Brown JK, Frohlich DR, Rosell RC. The sweet potato or silverleaf whiteflies: biotypes of *Bemisia tabaci* or a species complex? Annu Rev Entomol. 1995;40:511–534.
2. Czosnek H, Ghanim M. *Bemisia tabaci* – tomato yellow leaf curl virus interaction causing worldwide epidemics, p. 51-67. *In* Thompson W (ed), The whitefly, *Bemisia tabaci* (Homoptera: Aleyrodidae) interaction with geminivirus-infected host plants, Springer, Dordrecht. 2011.
3. de Moraes LA, Muller C, Bueno RCOF, Santos A, Bello VH, de Marchi BR, Watanabe LFM, Marubayashi JM, Santos BR, Yuki VA, Takada HM, de Barros DR, Neves CG, da Silva FN, Gonçalves MJ, Ghanim M, Boykin L, Pavan MA, Krause-Sakate R. Distribution and phylogenetics of whiteflies and their endosymbiont relationships after the Mediterranean species invasion in Brazil. Sci Rep. 2018;8:14589.

4. Ramesh KB, Gambhir S, Gouda MNR, Sagar VD, Sabtharishi S. Differences in life history traits and demographic parameters of three Asian genetic groups of *Bemisia tabaci* (Aleyrodidae: Hemiptera). Sci Rep. 2025;15:35316.
5. Lefeuvre P, Martin DP, Harkins G, Lemey P. The spread of tomato yellow leaf curl virus from the Middle East to the world. PLoS Pathog. 2010;6:e1001164.
6. Shahmohammadi N, Mansourpour M, Golnaraghi A. Current challenges and future perspectives on detection of geminiviruses, p. 3-24. *In* Gaur RK, Sharma P, Czosnek H (eds), Geminivirus: Detection, Diagnosis and Management, Academic Press, London, UK. 2022.
7. Rojas MR, Macedo MA, Maliano MR, Soto-Aguilar M, Souza JO, Briddon RW, Kenyon L, Rivera Bustamante RF, Zerbini FM, Adkins S, Legg JP, Kvarnheden A, Wintermantel WM, Sudarshana MR, Peterschmitt M, Lapidot M, Martin DP, Moriones E, Inoue-Nagata AK, Gilbertson RL. 2018. World management of geminiviruses. Annu Rev Phytopathol. 2022; 56:637-677.
8. Abhary M, Patil B, Fauquet C. Molecular Biodiversity, Taxonomy, and Nomenclature of tomato yellow leaf curl-like viruses, p. 85–118. *In* Czosnek, H. (ed.), Tomato yellow leaf curl disease. Springer, Dordrecht, The Netherlands. 2007.
9. Péréfarres F, Thierry M, Becker N, Lefeuvre P, Reynaud B, Delatte H, Lett JM. Biological invasions of geminiviruses: case study of TYLCV and *Bemisia tabaci* in Reunion Island. Viruses 2012; 4:3665-3688.
10. Navot N, Pichersky E, Zeidan M, Zamir D, Czosnek H. Tomato yellow leaf curl virus: A whitefly-transmitted geminivirus with a single genomic component. Virology 1991; 185:151–161.
11. Antignus Y, Cohen S. Cloning of tomato yellow leaf curl virus (TYLCV) and the complete nucleotide sequence of a mild infectious clone. Phytopathol. 1994;84:707–712.

12. Czosnek H, Hariton-Shalev A, Sobol I, Gorovits R, Ghanim M. The incredible journey of begomoviruses in their whitefly vector. Viruses 2017;9:273.
13. Lemaitre B, Hoffmann J. The host defense of *Drosophila melanogaster*. Annu Rev Immunol. 2007;25:697-743.
14. Kim Y, Ahmed S, Stanley D, An C. Eicosanoid-mediated immunity in insects. Dev Comp Immunol. 2018;83:130–43.
15. Kim Y, Stanley D. Eicosanoids in insects, p. 307-339. *In* Atkinson P, Yamanaka N (eds.), Comprehensive molecular insect science, 2nd ed, vol. 2. Elsevier, London, UK. 2025.
16. Vatanparast M, Ahmed S, Lee DH, Hwang SH, Hammock B, Kim,Y. EpOMEs act as immune suppressors in a lepidopteran insect, *Spodoptera exigua*. Sci Rep. 2020;10:20183.
17. Hrithik HMT, Shahmohammadi N, Jin G, Lee DH, Singh N, Vik A, Hammock BD, Kim Y. Insect immune resolution with EpOME/DiHOME and its dysregulation by their analogs leading to pathogen hypersensitivity. Insect Biochem Mol Biol. 2024;168:104104.
18. Shahmohammadi N, Haraji S, Khan F, Sørskår AM, Ebrahimi Danielsen P, Vik A, Kim Y. Antagonistic control of intracellular signals by EpOMEs in hemocytes induced by $PGE_2$ and their chemical modification for a potent insecticide. PLoS ONE 2025;20:e0320488.
19. Mollah MMI, Kim Y. Virulent secondary metabolites of entomopathogenic bacteria genera, *Xenorhabdus* and *Photorhabdus*, inhibit phospholipase $A_2$ to suppress host insect immunity. BMC Microbiol. 2020;20:359.
20. Shi YM, Hirschmann M, Shi YN, Ahmed S, Abebew D, Tobias NJ, Grün P, Crames JJ, Pöschel L, Kuttenlochner W, Richter C, Herrmann J, Müller R, Thanwisai A, Pidot SJ, Stinear TP, Groll M, Kim Y, Bode HB. Global analysis of biosynthetic gene clusters reveals conserved and unique natural products in entomopathogenic nematode-symbiotic bacteria. Nat Chem. 2022;14:701-712.

21. Jin G, Jeong JS, Kim IH, Kim Y. Suppression of a transcriptional regulator, HexA, is essential for triggering the bacterial virulence of the entomopathogen, *Xenorhabdus hominickii*. J Invertebr Pathol. 2024;207:108219.
22. Kim CY, Ahmed S, Stanley D, Kim Y. HMG-like DSP1 is a damage signal to mediate the western flower thrips, *Frankliniella occidentalis*, immune responses to tomato spotted wilt virus infection. Dev Comp Immunol. 2023;144:104706.
23. Shahmohammadi N, Khan F, Jin G, Kwon M, Lee D, Kim Y. TSWV suppresses the antiviral response of the insect vector, *Frankliniella occidentalis*, by elevating an immunosuppressive C18 oxylipin level using its virulent factor, NSs. Cells. 2024;13:1377.
24. Esmaeily M, Kim Y. Four phospholipase $A_2$ genes encoded in the western flower thrips genome and their functional differentiation in mediating development and immunity. Sci Rep. 2024;14:9766.
25. Shahmohammadi N, Esmaeily M, Abdisa E, Mandal E, Kim Y. Enhanced viral virulence by inhibition of EpOME biosynthesis in lepidopteran insects. J Invertebr Pathol. 2024;204:108095.
26. Friedmann M, Lapidot M, Cohen S, Pilowsky M. A novel source of Resistance to tomato yellow leaf curl virus exhibiting a symptomless reaction to viral infection. Am Soc Hortic Sci. 1998;123:1004–1007.
27. Livak KJ, Schmittgen TD. Analysis of relative gene expression data using real-time quantitative PCR and the $2^{-\Delta\Delta CT}$ method. Methods. 2001;25:402–408.
28. Tamura K, Stecher G, Kumar S. MEGA11: Molecular evolutionary genetics analysis version 11. Mol Biol Evol. 2021;38:3022–3027.
29. Wang XW, Blanc S, Ghanim M. Insect transmission of plant viruses: multilevel interactions optimize viral propagation. Annu Rev Phytopathol. 2020;58:35–55.

30. Pakkianathan BC, Kontsedalov S, Lebedev G, Mahadav A, Zeidan M, Czosnek H, Ghanim M. Replication of tomato yellow leaf curl virus in its whitefly vector, *Bemisia tabaci*. J Virol. 2015;89:9791-803.
31. He YZ, Wang YM, Yin TY, Fiallo-Olivé E, Liu YQ, Hanley-Bowdoin L, Wang XW. A plant DNA virus replicates in the salivary glands of its insect vector via recruitment of host DNA synthesis machinery. Proc Natl Acad Sci USA. 2020;117:16928-16937.
32. Kingsolver MB, Huang Z, Hardy RW. Insect antiviral innate immunity: pathways, effectors, and connections. J Mol Biol. 2013;425:4921-4936.
33. Xia WQ, Liang Y, Chi Y, Pan LL, Zhao J, Liu SS, Wang XW. Intracellular trafficking of begomoviruses in the midgut cells of their insect vector. PLoS Pathog. 2018;14:e1006866.
34. Zhao J, Lei T, Zhang XJ, Yin TY, Wang XW, Liu SS. A vector whitefly endocytic receptor facilitates the entry of begomoviruses into its midgut cells via binding to virion capsid proteins. PLoS Pathog. 2020;16:e1009053.
35. Wang S, Guo H, Ge F, Sun Y. Apoptotic neurodegeneration in whitefly promotes the spread of TYLCV. eLife 2020;9:e56168.
36. Wang X, Wang C, Ban F, Ghanim M, Pan L, Qian L, Liu Y, Wang X, Liu S. Apoptosis in a whitefly vector activated by a begomovirus enhances viral transmission. mSystems. 2020;5:10.
37. Kuzminsky I, Ghanim M. Immunity responses as checkpoints for efficient transmission of begomoviruses by whiteflies. Virology. 2025;605:110462.
38. Hildreth K, Kodani SD, Hammock BD, Zhao L. Cytochrome P450-derived linoleic acid metabolites EpOMEs and DiHOMEs: a review of recent studies. J Nutr Biochem. 2020;86:108484.

905 39. Xu J, Morisseau C, Hammock BD. Expression and characterization of epoxide hydrolase
906 from *Anopheles gambiae* with high activity on epoxy fatty acids. Insect Biochem Mol Biol.
907 2014;54:42-52.
908 40. Medzhitov R, Janeway C. Innate Immunity: The virtues of a nonclonal system of recognition.
909 Cell. 1997;91:295-298.
910 41. Kim CH, Park JW, Ha NC, Kang HJ, Lee BL. Innate immune response in insects:
911 recognition of bacterial peptidoglycan and amplification of its recognition signal. BMB Rep.
912 2008;41:93-101.
913 42. Ding TB, Li J, Chen EH, Niu JZ, Chu D. Transcriptome profiling of the whitefly *Bemisia*
914 *tabaci* MED in response to single infection of tomato yellow leaf curl virus, tomato chlorosis
915 virus, and their co-infection. Front Physiol. 2019;10:302.
916 43. Lu DY, Liao JY, Fajar A, Chen JB, Wei Y, Zhang ZH, Zhang Z, Zheng LM, Tan XQ, Zhou
917 XG, Shi XB, Liu Y, Zhang DY. Co-infection of TYLCV and ToCV increases cathepsin B
918 and promotes ToCV transmission by *Bemisia tabaci* MED. Front Microbiol.
919 2023;14:1107038.
920 44. Bulet P, Stöcklin R, Menin L. Anti-microbial peptides: from invertebrates to vertebrates.
921 Immunol Rev. 2004;198:169-184.
922 45. Ayres JS, Schneider DS. Tolerance of Infections. Annu Rev Immunol. 2012;30:271-294.
923 46. Wang X, Zafar J, Yang X, De Mandal S, Hong Y, Jin F, Xu X. Gut bacterium *Burkholderia*
924 *cepacia* (BsNLG8) and immune gene defensin A contribute to the resistance against
925 nicotine-induced stress in *Nilaparvata lugens* (Stal). Ecotoxicol Environ Saf.
926 2024;277:116371.
927 47. Hariton Shalev A, Sobol I, Ghanim M, Liu SS, Czosnek H. The whitefly *Bemisia*
928 *tabaci knottin-1* gene is implicated in regulating the quantity of tomato yellow leaf curl virus

ingested and transmitted by the insect. Viruses 2016;8:205.

48. Stanley D, Kim Y. Prostaglandins and other eicosanoids in insects: biosynthesis and biological actions. Front Physiol. 2019;9:1927.

49. Li P, Liu C, Deng WH, Yao DM, Pan LL, Li YQ, Liu YQ, Liang Y, Zhou XP, Wang XW. Plant begomoviruses subvert ubiquitination to suppress plant defenses against insect vectors. PLoS Pathog. 2019;15:e1007607.

50. Guerrero J, Regedanz E, Lu L, Ruan J, Bisaro DM, Sunter G. Manipulation of the plant host by the geminivirus AC2/C2 protein, a central player in the infection cycle. Front Plant Sci. 2020;11:591.

51. Li P, Zhang L, Yan XT, Zheng C, Zhang XY, Chen JP, Liu SS, Wang XW. Suppression of TGA2-mediated salicylic acid defense by tomato yellow leaf curl virus C2 via disruption of TCP7-like transcription factor activity in tobacco. Plant Cell Environ. 2025;48:4039-4050.

52. Shahmohammadi N, Khan F, Lee D, Lee D, Kim Y. Wild-type and resistance-breaking strains of tomato spotted wilt virus differentially upregulate the immunosuppressive epoxyoctadecamonoenoic acid biosynthesis of its insect vector, *Frankliniella occidentalis*. J Gen Virol. 2025;106:002175.

53. Wang Y, He Y, Ye X, Guo T, Pan L, Liu S, Ng JCK, Wang X. A balance between vector survival and virus transmission is achieved through JAK/STAT signaling inhibition by a plant virus. Proc Natl Acad Sci USA. 2022;119:e2122099119.

## Figure captions

**Fig. 1** TYLCV accumulation in the intestine of *B. tabaci* and alteration of host metabolism. (**A**) Progressive increase in TYLCV accumulation in the intestine of *B. tabaci*. Viral localization was monitored by fluorescence in situ hybridization (FISH) in intestinal tissues of adult whiteflies at 6, 12, 24, and 48 h after virus acquisition. Adult *B. tabaci* acquired TYLCV by feeding on infected tomato plants for 24 h, and intestinal tissues were dissected at the indicated time points for FISH analysis. 'Ca', caeca; 'FG', foregut; 'MG', midgut; 'HG', hindgut. The intestine was visualized using differential interference contrast (DIC), and TYLCV signals were detected using fluorescein isothiocyanate (FITC) under a fluorescence microscope (DM2500; Leica, Wetzlar, Germany). The experiment was replicated three times with three independent adult insects. Scale bar = 0.1 mm. Non-virulent control did not show any fluorescence. (**B**) Comparative expression profiles of genes involved in different metabolic pathways using KEGG analysis between viruliferous and non-viruliferous whiteflies. Expression levels are presented as log-transformed transcripts per million (log TPM). The full gene names of the abbreviated accessions are listed in Supplementary Table S4.

**Fig. 2** Opposite roles of two oxylipins ($PGE_2$ and EpOME) in manipulating TYLCV multiplication. (**A**) A diagram indicating the biosynthetic pathways for the oxylipins. Phospholipid ('PL') is catalyzed by phospholipase $A_2$ ('$PLA_2$') to release linoleic acid ('LA'). LA is then oxygenated by cytochrome P450 monooxygenase ('CYP') to produce EpOME, which is degraded into DiHOME by soluble epoxide hydroxylase ('sEH'). LA is also elongated and desaturated by elongase ('ELO') and desaturase ('DES'), respectively, to produce arachidonic acid ('AA'). AA is then further oxygenated to different prostaglandins (PGs) by

$PGD_2$ synthase ('PGDS'), $PGE_2$ synthase ('PGES'), and $PGF_{2\alpha}$ synthase ('PGFS'). (**B**) Effects of oxylipin precursors (AA and LA) on TYLCV accumulation in the intestine assessed by FISH. The intestine was visualized using differential interference contrast ('DIC'), and TYLCV signals were detected using fluorescein isothiocyanate ('FITC') under a fluorescence microscope (DM2500; Leica, Wetzlar, Germany): 'Ca' for caeca, 'MG' for midgut, and 'HG' for hindgut. Scale bar = 0.1 mm. (**C**) Effects of AA and LA on TYLCV accumulation assessed by qPCR at 24 h after treatment. Viral titers were quantified in a whole sample consisting of 20 individual adults with three independent samplings. (**D**) Effects of AA and LA on TYLCV accumulation assessed by immunofluorescence assay using a specific antibody to TYLCV coat protein at 24 h after treatment. For quantification of the signal intensity, each replication used individual adult with three independent replications per treatment. (**E**) Effects of three different PGs (0.1 μg/mL) on TYLCV accumulation assessed by qPCR at 24 h after treatment. (**F**) Effects of two EpOMEs (0.1 μg/mL) on TYLCV accumulation assessed by qPCR at 24 h after treatment. All compounds were administered to adult whiteflies by a membrane feeding together with TYLCV. 'DMSO' represents a solvent control. At 24 h after treatment, TYLCV titers were quantified by qPCR. Viral titers were quantified in a whole sample consisting of 20 individual adults with three independent samplings. Different letters above the standard deviation bars indicate significant differences among treatments at Type I error = 0.05 (LSD test).

**Fig. 3** Phospholipase $A_2$ ($PLA_2$) genes of *B. tabaci* and their antiviral activity against TYLCV. (**A**) Influence of three inhibitors (1 μg/mL) specific to eicosanoid biosynthesis on TYLCV accumulation in *B. tabaci*: dexamethasone ('DEX') specific to $PLA_2$, naproxen ('NAP') specific to cyclooxygenase ('COX'), and esculetin ('ESC') specific to lipoxygenase. 'DMSO'

represents solvent control. Each treatment consisted of three biological replicates, each containing 20 adult whiteflies. (**B**) A phylogenetic analysis of four $PLA_2$ genes (*$BtPLA_2$-A* ~ *$BtPLA_2$-D*) encoded in the *B. tabaci* genome, along with other $PLA_2$ genes separately identified into 15 Groups (I-XV), which are also classified into five different $PLA_2$ types: secretory ($sPLA_2$), lysosomal ($LPLA_2$), lipoprotein-associated ($LpPLA_2$), $Ca^{2+}$-independent cellular ($iPLA_2$), and $Ca^{2+}$-dependent cellular ($cPLA_2$). (**C**) Developmental expression profiles of the four $PLA_2$ genes from egg to adult. 'N1-N3' represents three nymphal instars. (**D**) Influence of TYLCV infection on the expression levels of the four $PLA_2$ genes. qPCR analysis was performed at 24 h after viral infection using three biological replicates, each containing 20 adult whiteflies. (**E**) Effects of four individual RNA interference (RNAi) treatments using gene-specific dsRNAs ($dsPLA_2$-A ~ $dsPLA_2$-D, 500 μg/mL) against the four $PLA_2$ genes on TYLCV titers of the viruliferous adults. 'dsCON' indicates a control dsRNA. After 24 h, the viral titers were quantified by qPCR using three biological replicates, each containing 20 adult whiteflies. Different letters or asterisks above the standard deviation bars indicate significant differences among treatments at Type I error = 0.05 (LSD test). 'ns' represents no significant difference.

**Fig. 4** $PGE_2$ synthase (Bt-PGES2)/receptor (Bt-$PGE_2R$) of *B. tabaci* and their antiviral activities against TYLCV. (**A**) A diagram indicating an antiviral pathway of $PGE_2$, in which $PGE_2$ is synthesized from $PGD_2$ by PGES2 and mediates an antiviral response via its $PGE_2R$. (**B**) Phylogenetic analyses of *Bt-PGES* and *Bt-$PGE_2R$* encoded in the *B. tabaci* genome along with their orthologous genes. (**C**) Developmental expression profiles of the two genes from egg to adult. 'N1-N3' represents three nymphal instars. (**D**) Up-regulation of the two genes in response to TYLCV infection. (**E**) Influence of two individual RNA interference (RNAi) treatments using gene-specific dsRNAs (dsPGES and ds$PGE_2R$, 500 μg/mL) against *Bt-PGES*

or *Bt-PGE$_2$R* genes on TYLCV titers of the viruliferous adults. 'dsCON' indicates a control dsRNA. After 24 h, the viral titers were quantified by qPCR using three biological replicates, each containing 20 adult whiteflies. Different letters or asterisks above the standard deviation bars indicate significant differences among treatments at Type I error = 0.05 (LSD test).

**Fig. 5** Up-regulation of EpOME levels in viruliferous *B. tabaci* and proviral activity for TYLCV. (**A**) Quantification of EpOMEs using LC–MS/MS. Two EpOME peaks are denoted in the chromatograms. EpOME levels were quantified from three independent biological replicates, each consisting of 200 pooled viruliferous/non-viruliferous adult *B. tabaci* samples. Data are presented as mean ± SD of three biological replicates. (**B**) Proviral activity of EpOME for TYLCV. An inhibitor ('AUDA', 10 μg/mL) specific to soluble epoxide hydrolase ('sEH') or an EpOME analog (AS56, 0.1 μg/mL) was fed to the viruliferous *B. tabaci*. 'DMSO' represents a solvent control. After 24 h, the viral titers were quantified by qPCR using three biological replicates, each containing 20 adult whiteflies. Different letters or asterisks above the standard deviation bars indicate significant differences among treatments at Type I error = 0.05 (LSD test).

**Fig. 6** Cytochrome P450 monooxygenases (Bt-CYPs) of *B. tabaci* and their proviral activities for TYLCV. (**A**) Phylogenetic analysis of 44 *Bt-CYP* genes encoded in the *B. tabaci* genome, along with other EpOME synthases (*Fo-CYP24*, *Se-CYP32*, and *Hs-CYP2*). (**B**) Developmental expression profiles of the three CYP genes from egg to adult. 'N1-N3' represents three nymphal instars. (**C**) Influence of TYLCV infection on the expression levels of the three *CYP* genes. qPCR analysis was performed at 24 h after viral infection using three biological replicates, each containing 20 adult whiteflies. (**D**) Influence of three individual RNA interference (RNAi)

1044 treatments using gene-specific dsRNAs (dsBt-CYP5 ~ dsBt-CYP7, 500 μg/mL) against the
1045 three CYP genes on TYLCV titers of the viruliferous adults. 'dsCON' indicates a control
1046 dsRNA. After 24 h, the viral titers were quantified by qPCR using three biological replicates,
1047 each containing 20 adult whiteflies. Different letters or asterisks above the standard deviation
1048 bars indicate significant differences among treatments at Type I error = 0.05 (LSD test).
1049
1050 **Fig. 7** An EpOME-degrading enzyme, soluble epoxide hydrolase (Bt-sEH) of *B. tabaci* and its
1051 proviral activities for TYLCV. (**A**) Phylogenetic analysis of four epoxide hydrolase (*Bt-sEH1*
1052 *~ sEH3, Bt-JHEH*) genes encoded in the *B. tabaci* genome along with other sEH and JHEH
1053 genes. (**B**) Developmental expression profiles of the four epoxide hydrolase genes from egg to
1054 adult. 'N1-N3' represents three nymphal instars. (**C**) Influence of TYLCV infection on the
1055 expression levels of the four epoxide hydrolase genes. qPCR analysis was performed at 24 h
1056 after viral infection using three biological replicates, each containing 20 adult whiteflies. (**D**)
1057 Influence of three individual RNA interference (RNAi) treatments using gene-specific dsRNAs
1058 (ds-sEH1 ~ ds-sEH3, 500 μg/mL) against the three *sEH* genes on TYLCV titers of the
1059 viruliferous adults. 'dsCON' indicates a control dsRNA. After 24 h, the viral titers were
1060 quantified by qPCR using three biological replicates, each containing 20 adult whiteflies.
1061 Different letters or asterisks above the standard deviation bars indicate significant differences
1062 among treatments at Type I error = 0.05 (LSD test).
1063
1064 **Fig. 8** Temporal regulation of two oxylipin biosynthesis pathways in *B. tabaci* after TYLCV
1065 infection. Expression analyses were performed for seven days after viral infection of three
1066 genes (*$BtPLA_2$-A*, *$BtPLA_2$-C*, and *Bt-PGES2*) for $PGE_2$ biosynthesis and three other genes (*Bt-*
1067 *CYP6*, *Bt-sEH2*, and *Bt-sEH3*) for EpOME biosynthesis. qPCR analysis was performed using

three biological replicates, each containing 20 adult whiteflies. Different letters above the standard deviation bars indicate significant differences among treatments in each gene at Type I error = 0.05 (LSD test).

**Fig. 9** Differential control of EpOME synthetic machinery expression by two TYLCV strains (TYLCV-IL and TYLCV-Mld). (**A**) Difference in virulence between the two viral strains with respect to disease symptoms and severity after 30 days post-infection. Viruliferous *B. tabaci* after 48 h AAP were used to inoculate healthy tomato plants. (**B**) TYLCV accumulation in the intestine of *B. tabaci* by FISH analysis under differential interference contrast ('DIC') and fluorescein isocyanate ('FITC'): 'Ca' for caeca, 'MG' for midgut, and 'HG' for hindgut. Each treatment consisted of one individual adult, with three independent biological replicates. Scale bars represent 0.1 mm. Viral titers were assessed in FITC intensity normalized by the DAPI signal intensity in the intestine. In addition, the viral titers were assessed by qPCR from the whole-body samples for seven days post-infection. qPCR analysis was performed using three biological replicates, each containing 50 adult whiteflies. Different letters above the standard deviation bars indicate significant differences among treatments at Type I error = 0.05 (LSD test). (**C**) Differential effect of the two TYLCV strains on modulating expressions of EpOME synthetic (*Bt-CYP6*) and degrading (*Bt-sEH2* and *Bt-sEH3*) genes. qPCR analysis was performed at 24 h after viral infection using three biological replicates, each containing 20 adult whiteflies. Different letters above standard deviation bars indicate significant differences among means at Type I error = 0.05 (LSD test).

**Fig. 10** Apoptosis in the intestine of *B. tabaci* as a proviral response to TYLCV. (**A**) Opposite roles of two oxylipins ($PGE_2$ and EpOME, each 0.1 μg/mL) in inducing intestinal apoptosis of

*B. tabaci* upon TYLCV-IL infection assessed by a TUNEL assay. The intestine was visualized at 24 h after viral infection using differential interference contrast ('DIC'), and apoptotic signals were detected using fluorescein isothiocyanate ('FITC') under a fluorescence microscope (DM2500; Leica, Wetzlar, Germany): 'Ca' for caeca, 'MG' for midgut, and 'HG' for hindgut. Each treatment consisted of one individual adults, with three independent biological replicates. Scale bar = 0.1 mm. Apoptosis quantification was assessed as FITC intensity normalized by the intensity of DAPI signal intensity in the intestine. 'DMSO' represents a solvent control. (**B**) Differential effect of two TYLCV strains on the expressions of an initiator ('Dronc', a target of inhibitor of apoptosis ('IAP')) and an effector ('Cas 1') caspases in viruliferous *B. tabaci*. qPCR analysis was performed at 24 h after viral infection using three biological replicates, each containing 20 adult whiteflies. (**C**) Effect of $PGE_2$ and EpOME (0.1 μg/mL) in inducing intestinal apoptosis of *B. tabaci* upon TYLCV-IL infection assessed by an immunofluorescence assay using cleaved caspase-3 (Asp175) specific antibody. The intestine was visualized at 24 h after treatment and apoptotic signals were detected using FITC under the fluorescence microscope. Each replication used individual adult and was independently replicated three times. Scale bar = 0.1 mm. (**D**) Influence of an apoptosis inhibitor ('Z-VAD', 50 μM) on the viral titer of TYLCV-IL or TYLCV-Mld in viruliferous *B. tabaci*. Relative TYLCV titers were measured by qPCR at 24 h post-infection using three biological replicates, each containing 20 adult whiteflies. Different letters above standard deviation bars indicate significant differences among means at Type I error = 0.05 (LSD test).

**Fig. 11** Selective control of proviral and antiviral immunity-associated genes of *B. tabaci* by EpOME. (**A**) Influence of 12,13- EpOME (0.1 μg/mL) or $PGE_2$ (0.1 μg/mL) addition on the expressions of the six immune-associated genes at 24 h post-treatment in viruliferous *B. tabaci*.

qPCR analysis was performed using three biological replicates, each containing 20 adult whiteflies. (**B**) Influence of individual RNAi treatments specific to six immunity-associated genes (*Defensin*, *knottin*, *PGRP*, *cathepsin B* (*Cath-B*), *cathepsin F* (*Cath-F*), and *cathepsin L* (*Cath-L*)) on the TYLCV titer in viruliferous *B. tabaci*. Individual dsRNA (500 μg/mL) against each of the immune-associated genes of *B. tabaci* were administered to adults by feeding along with TYLCV-IL. TYLCV titer was measured by qPCR using three biological replicates, each containing 20 adult whiteflies. Different letters above standard deviation bars indicate significant differences among means at Type I error = 0.05 (LSD test).

**Fig. 12** TYLCV-C2 as a virulent factor for manipulating host EpOME biosynthesis in *B. tabaci*. (**A**) TYLCV genome indicating six viral genes (V1-V2 and C1-C4) between intergenic region (IR) at both ends. (**B**) Effects of individual RNAi treatments (dsRNA$^{V1}$, dsRNA$^{V2}$, dsRNA$^{C1}$, dsRNA$^{C2}$, dsRNA$^{C3}$, and dsRNA$^{C4}$) specific to six viral genes, on the expression levels of *Bt-CYP6*, *Bt-sEH2*, and *Bt-sEH3* at 24 h post-RNAi treatment. 'dsCON' indicates a control dsRNA. TYLCV-IL was administered to adults, and the gene expression levels were assessed by qPCR using three biological replicates, each containing 20 adult whiteflies. (**C**) Rescue effect of the suppressed viral titer induced by RNAi specific to TYLCV-C2 by EpOME addition. Each treatment was replicated three times, each containing 20 adult whiteflies. Distinct letters above the standard error bars signify significant differences among the means at a Type I error rate of 0.05 (LSD test).

**Fig. 13** A working model of exploiting host EpOME for TYLCV accumulation in *B. tabaci*. Upon acquisition of TYLCV by the whitefly, TYLCV-C2 induces EpOME biosynthesis by inducing *Bt-CYP* expression while suppressing *Bt-sEH* expression. Up-regulated EpOME

levels induce proviral factors but suppress antiviral factors, leading to a reshaping the physiological conditions of *B. tabaci* to facilitate TYLCV multiplication.

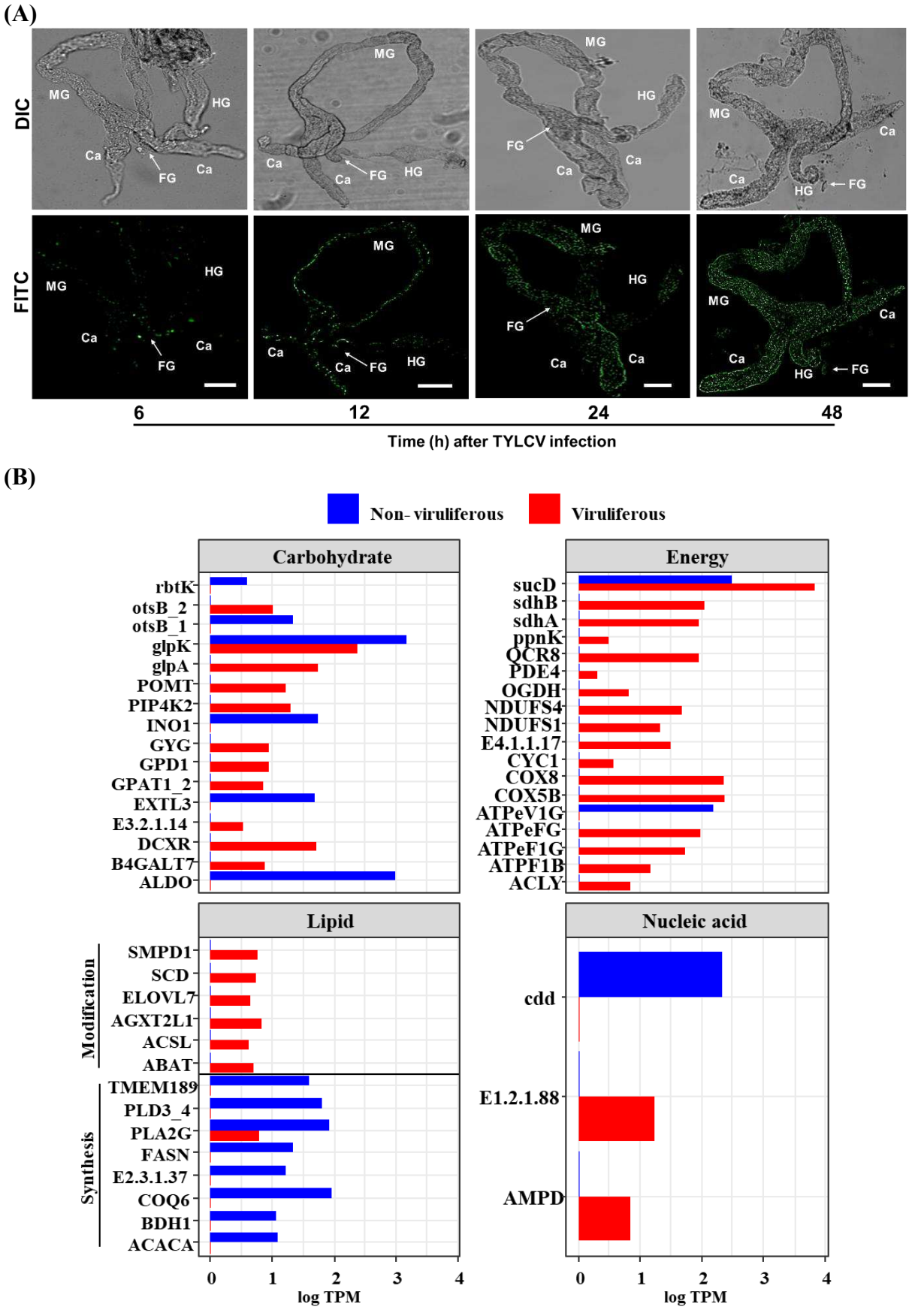
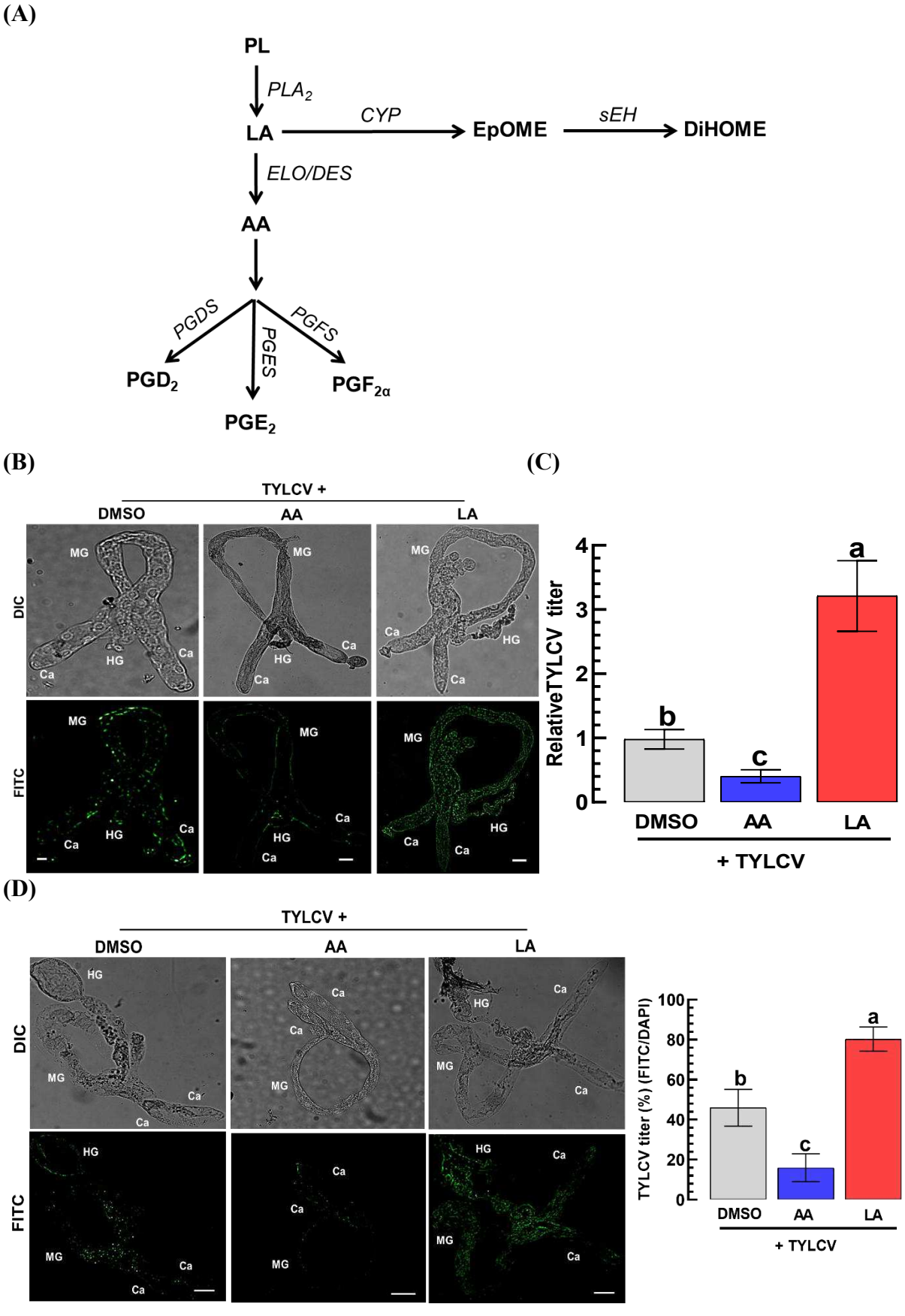

(A)
DIC
FITC
MG
HG
Ca
FG
6
12
24
48
Time (h) after TYLCV infection
(B)
Non- viruliferous
Viruliferous
Carbohydrate
rbtK
otsB_2
otsB_1
glpK
glpA
POMT
PIP4K2
INO1
GYG
GPD1
GPAT1_2
EXTL3
E3.2.1.14
DCXR
B4GALT7
ALDO
Energy
sucD
sdhB
sdhA
ppnK
QCR8
PDE4
OGDH
NDUFS4
NDUFS1
E4.1.1.17
CYC1
COX8
COX5B
ATPeV1G
ATPeFG
ATPeF1G
ATPF1B
ACLY
Lipid
Modification
SMPD1
SCD
ELOVL7
AGXT2L1
ACSL
ABAT
Synthesis
TMEM189
PLD3_4
PLA2G
FASN
E2.3.1.37
COQ6
BDH1
ACACA
Nucleic acid
cdd
E1.2.1.88
AMPD
0
1
2
3
4
log TPM

**Fig. 1**


(A)
PL
PLA2
LA
CYP
EpOME
sEH
DiHOME
ELO/DES
AA
PGDS
PGES
PGFS
PGD2
PGE2
PGF2α
(B)
TYLCV +
DMSO
AA
LA
DIC
FITC
MG
HG
Ca
(C)
RelativeTYLCV titer
0
1
2
3
4
a
b
c
DMSO
AA
LA
+ TYLCV
(D)
TYLCV +
DMSO
AA
LA
DIC
FITC
TYLCV titer (%) (FITC/DAPI)
0
20
40
60
80
100
a
b
c
DMSO
AA
LA
+ TYLCV

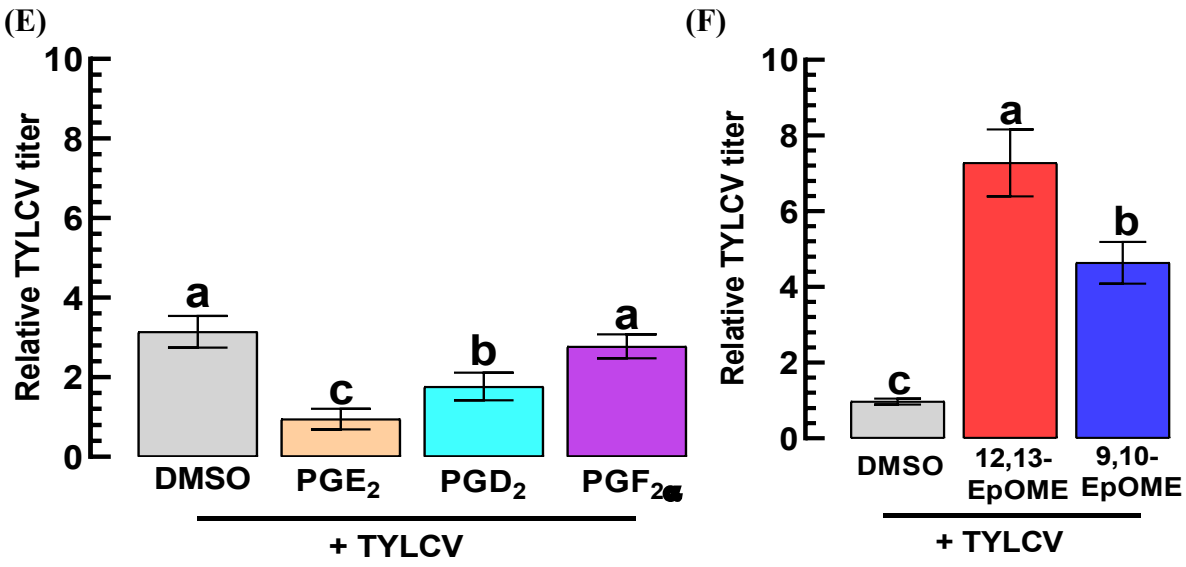
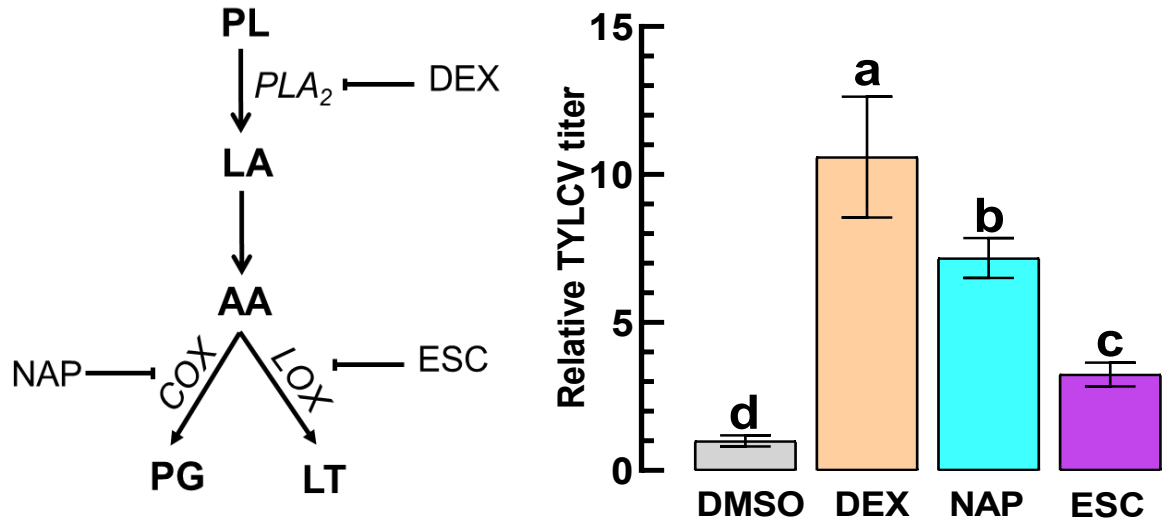
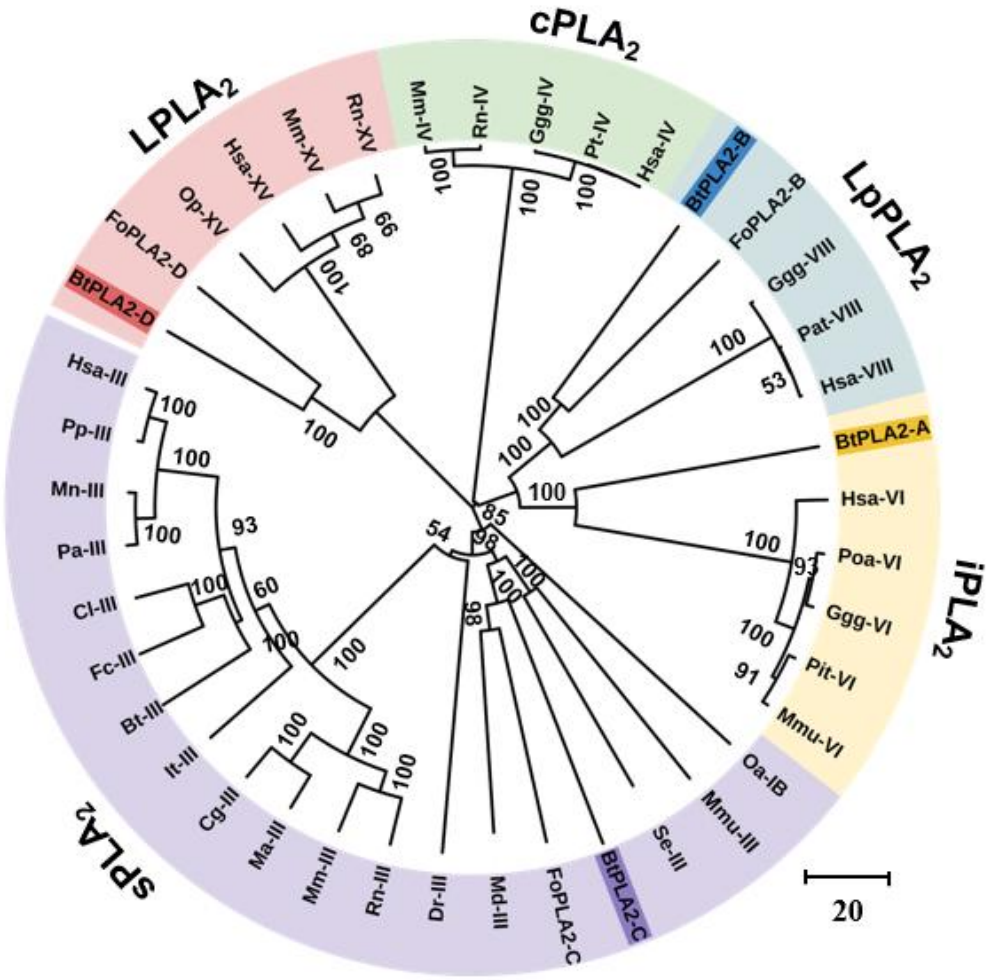

(E)
Relative TYLCV titer
10
8
6
4
2
0
a
c
b
a
DMSO
PGE2
PGD2
PGF2α
+ TYLCV
(F)
Relative TYLCV titer
10
8
6
4
2
0
c
a
b
DMSO
12,13-EpOME
9,10-EpOME
+ TYLCV

**Fig. 2**

**(A)**


PL
PLA2
DEX
LA
AA
NAP
COX
LOX
ESC
PG
LT
Relative TYLCV titer
15
10
5
0
a
b
c
d
DMSO
DEX
NAP
ESC

**(B)**


cPLA2
LPLA2
LpPLA2
iPLA2
sPLA2
Rn-XV
Mm-XV
Hsa-XV
Op-XV
FoPLA2-D
BtPLA2-D
Mm-IV
Rn-IV
Ggg-IV
Pt-IV
Hsa-IV
BtPLA2-B
FoPLA2-B
Ggg-VIII
Pat-VIII
Hsa-VIII
BtPLA2-A
Hsa-VI
Poa-VI
Ggg-VI
Pit-VI
Mmu-VI
Oa-IB
Mmu-III
Se-III
BtPLA2-C
FoPLA2-C
Md-III
Dr-III
Rn-III
Mm-III
Ma-III
Cg-III
It-III
Bt-III
Fc-III
Cl-III
Pa-III
Mn-III
Pp-III
Hsa-III
20

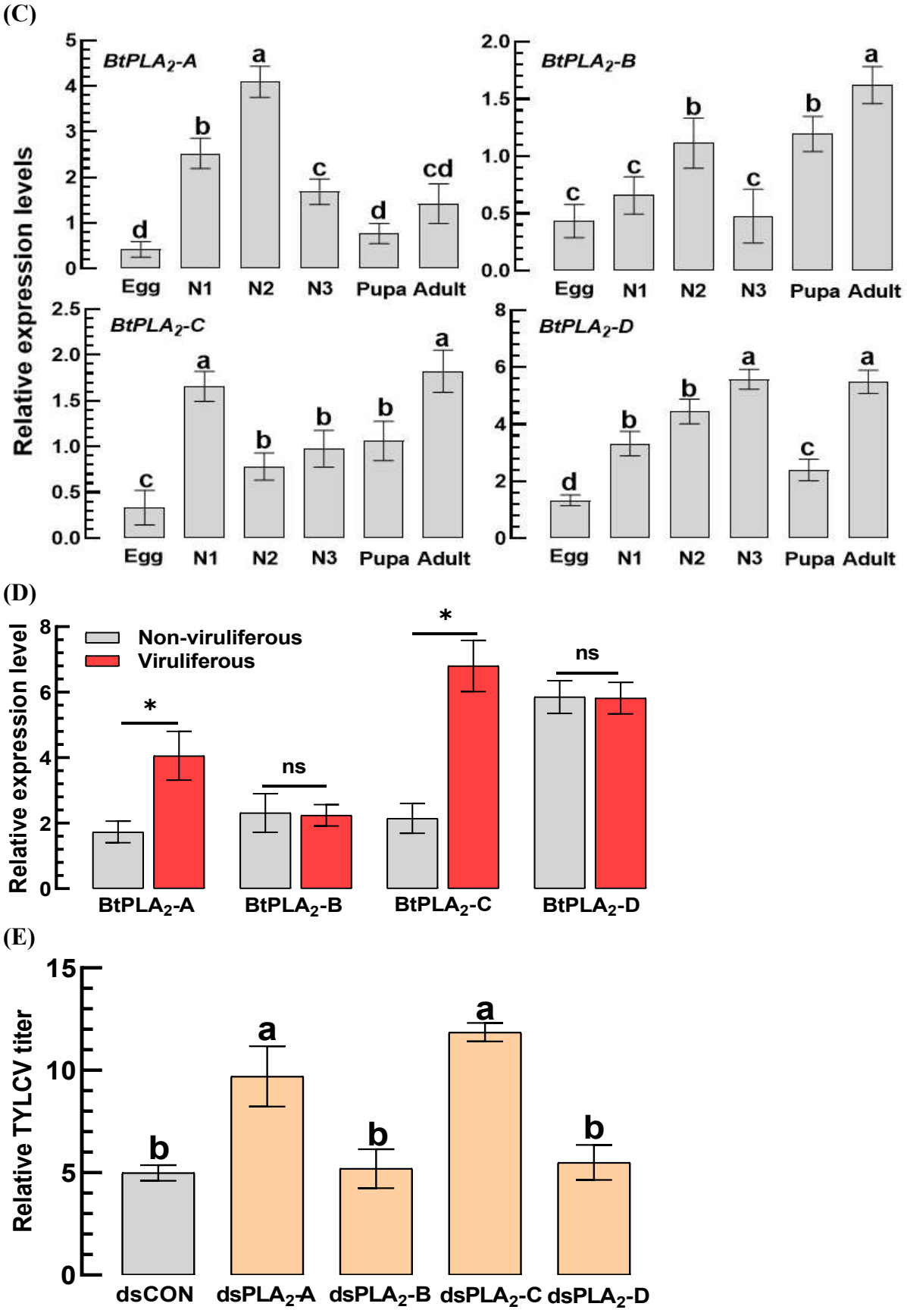
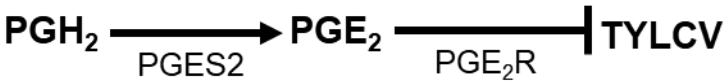
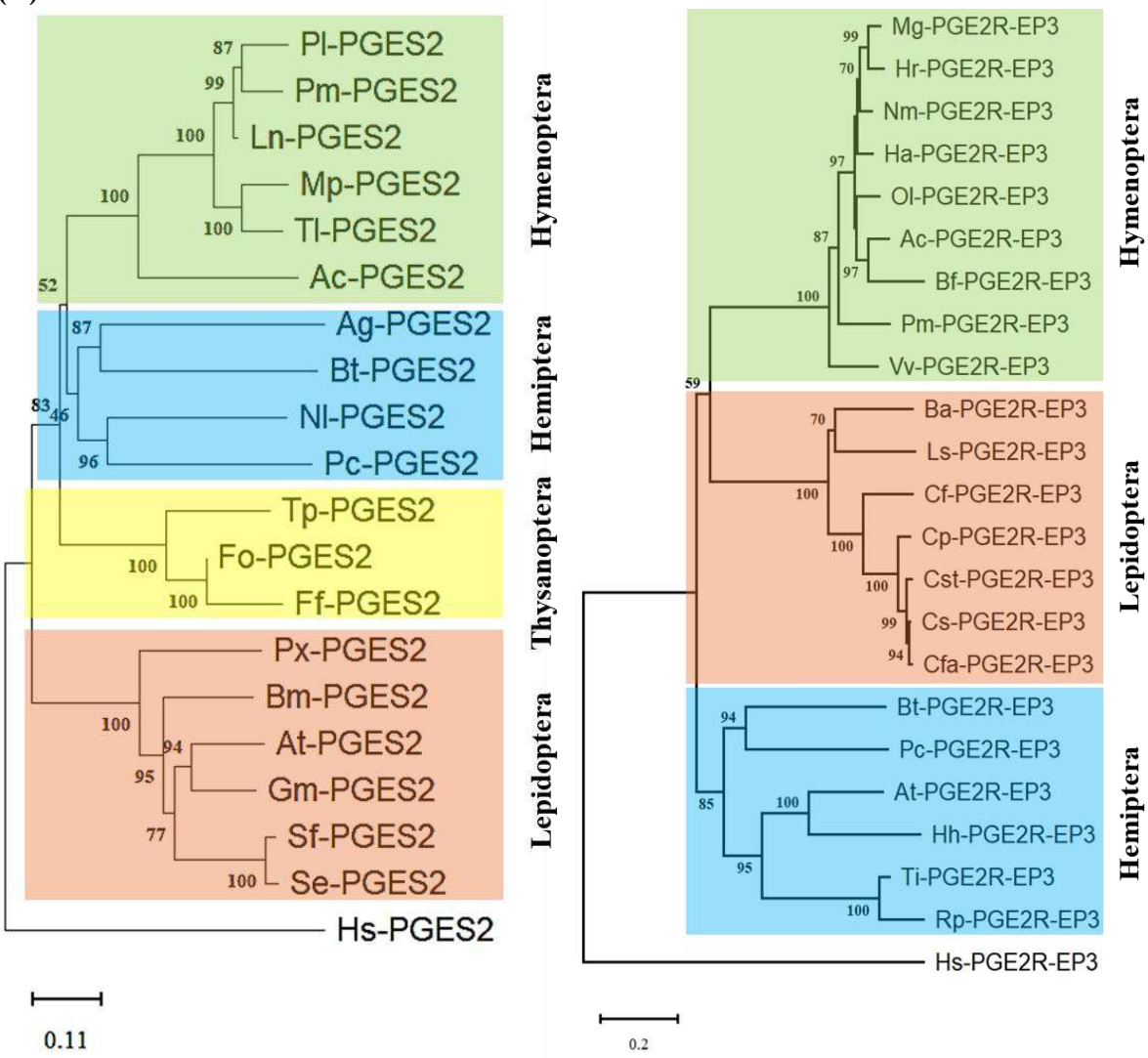

(C)
Relative expression levels
BtPLA2-A
BtPLA2-B
BtPLA2-C
BtPLA2-D
Egg
N1
N2
N3
Pupa
Adult
(D)
Relative expression level
Non-viruliferous
Viruliferous
*
ns
BtPLA2-A
BtPLA2-B
BtPLA2-C
BtPLA2-D
(E)
Relative TYLCV titer
dsCON
dsPLA2-A
dsPLA2-B
dsPLA2-C
dsPLA2-D

**Fig. 3**

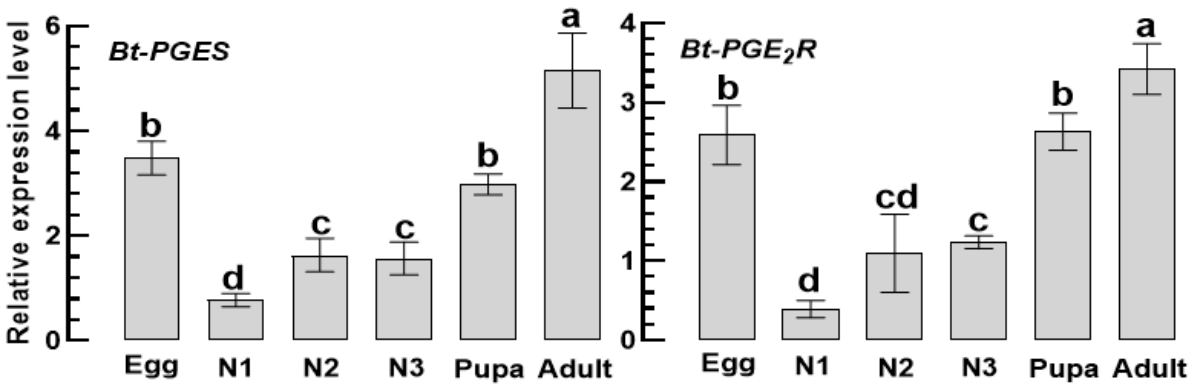
**(A)**


PGH2
PGES2
PGE2
PGE2R
TYLCV

**(B)**


Pl-PGES2
Pm-PGES2
Ln-PGES2
Mp-PGES2
Tl-PGES2
Ac-PGES2
Ag-PGES2
Bt-PGES2
Nl-PGES2
Pc-PGES2
Tp-PGES2
Fo-PGES2
Ff-PGES2
Px-PGES2
Bm-PGES2
At-PGES2
Gm-PGES2
Sf-PGES2
Se-PGES2
Hs-PGES2
0.11
Hymenoptera
Hemiptera
Thysanoptera
Lepidoptera
Mg-PGE2R-EP3
Hr-PGE2R-EP3
Nm-PGE2R-EP3
Ha-PGE2R-EP3
Ol-PGE2R-EP3
Ac-PGE2R-EP3
Bf-PGE2R-EP3
Pm-PGE2R-EP3
Vv-PGE2R-EP3
Ba-PGE2R-EP3
Ls-PGE2R-EP3
Cf-PGE2R-EP3
Cp-PGE2R-EP3
Cst-PGE2R-EP3
Cs-PGE2R-EP3
Cfa-PGE2R-EP3
Bt-PGE2R-EP3
Pc-PGE2R-EP3
At-PGE2R-EP3
Hh-PGE2R-EP3
Ti-PGE2R-EP3
Rp-PGE2R-EP3
Hs-PGE2R-EP3
0.2
Hymenoptera
Lepidoptera
Hemiptera

**(C)**


Relative expression level
Bt-PGES
Egg
N1
N2
N3
Pupa
Adult
Bt-PGE2R
Egg
N1
N2
N3
Pupa
Adult

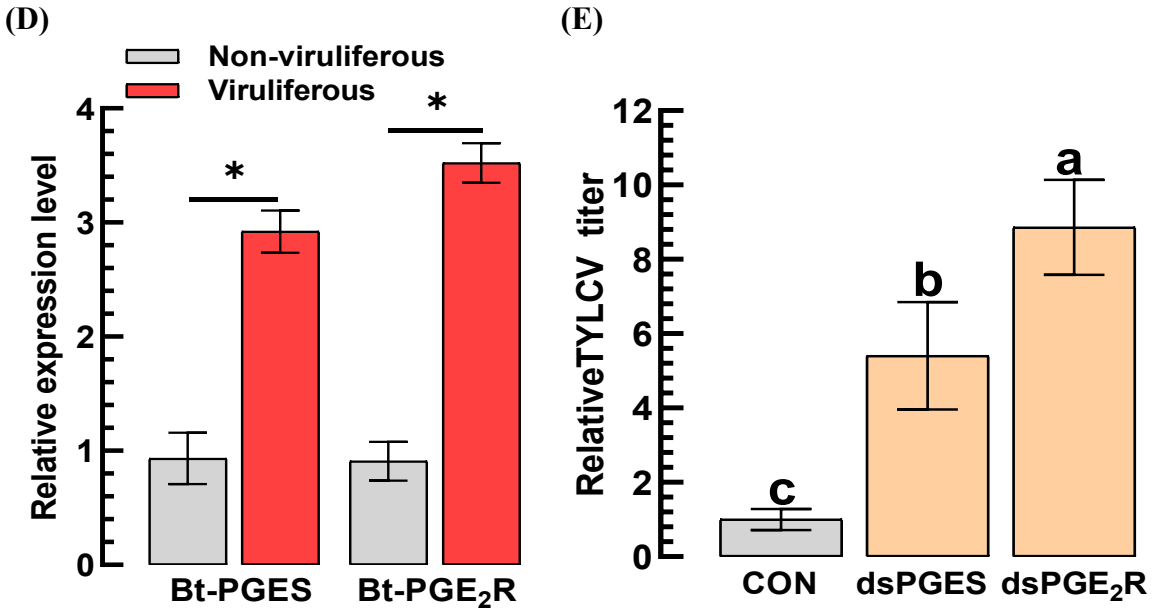
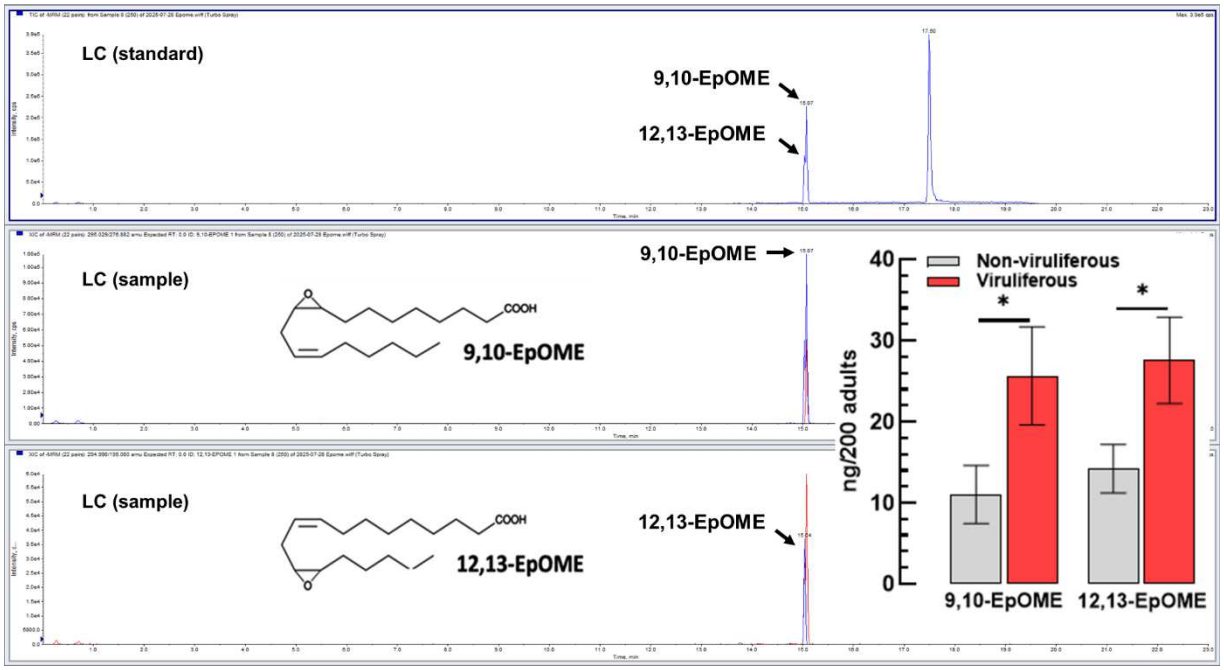

(D)
Non-viruliferous
Viruliferous
Relative expression level
0
1
2
3
4
*
*
Bt-PGES
Bt-PGE2R
(E)
RelativeTYLCV titer
0
2
4
6
8
10
12
c
b
a
CON
dsPGES
dsPGE2R

**Fig. 4**

**(A)**


LC (standard)
9,10-EpOME
12,13-EpOME
LC (sample)
9,10-EpOME
COOH
9,10-EpOME
LC (sample)
12,13-EpOME
COOH
12,13-EpOME
Non-viruliferous
Viruliferous
ng/200 adults
40
30
20
10
0
9,10-EpOME
12,13-EpOME

**(B)**

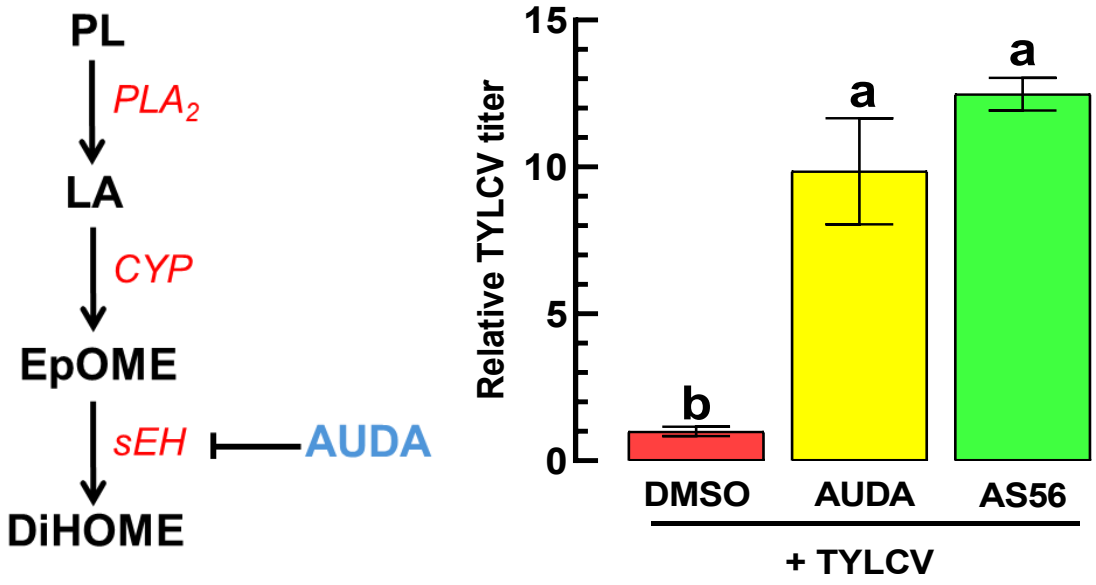

PL
PLA2
LA
CYP
EpOME
sEH
AUDA
DiHOME
Relative TYLCV titer
15
10
5
0
b
a
a
DMSO
AUDA
AS56
+ TYLCV

**Fig. 5**

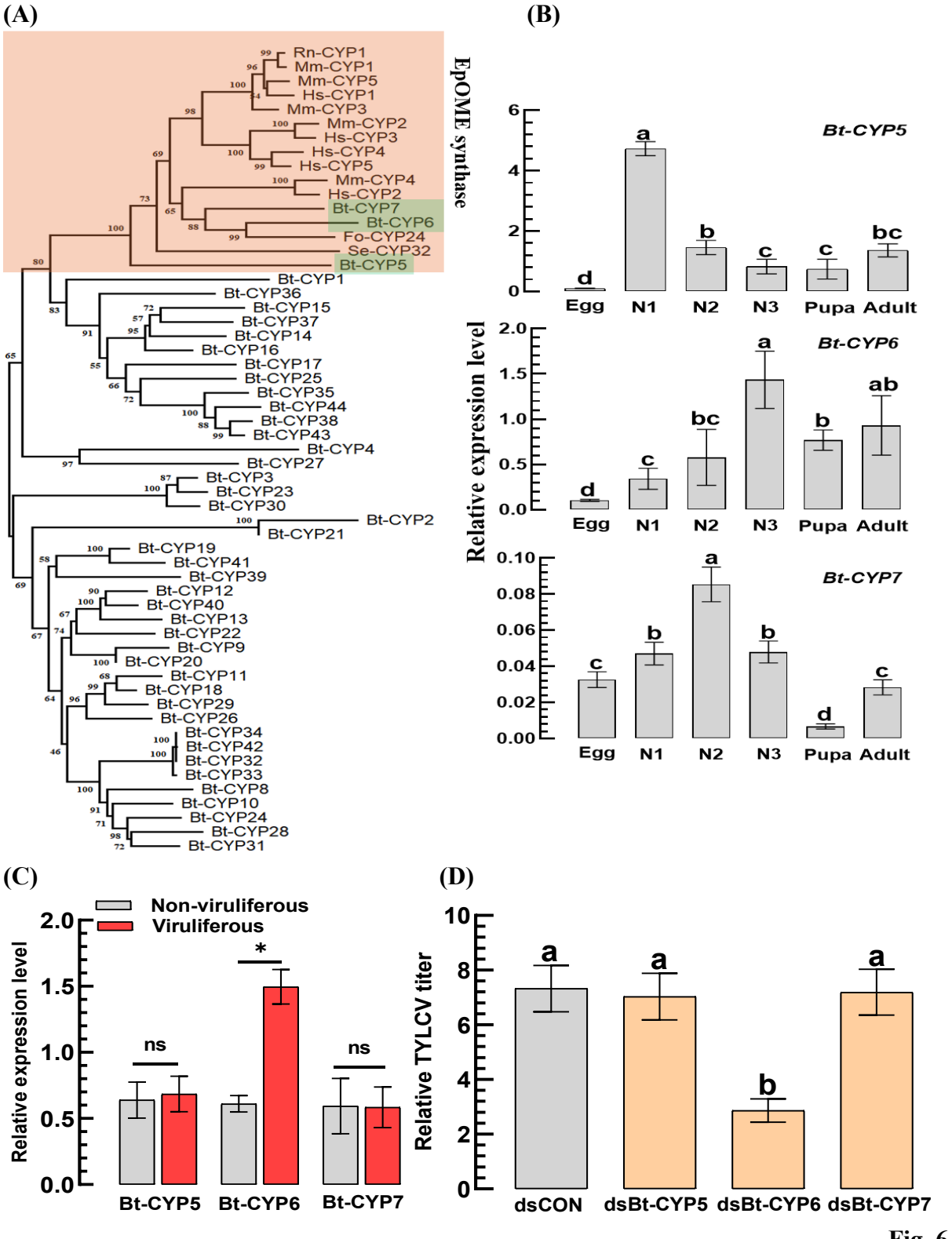
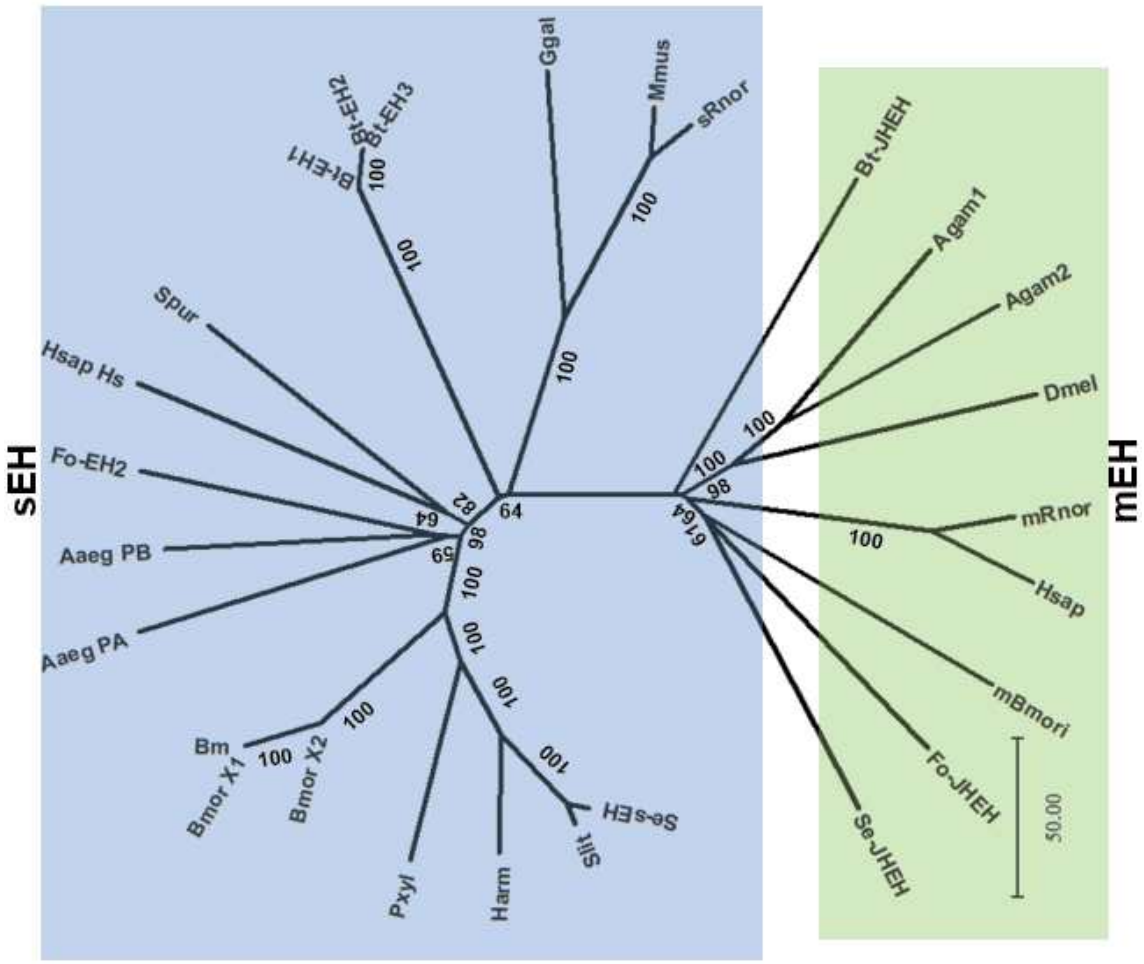
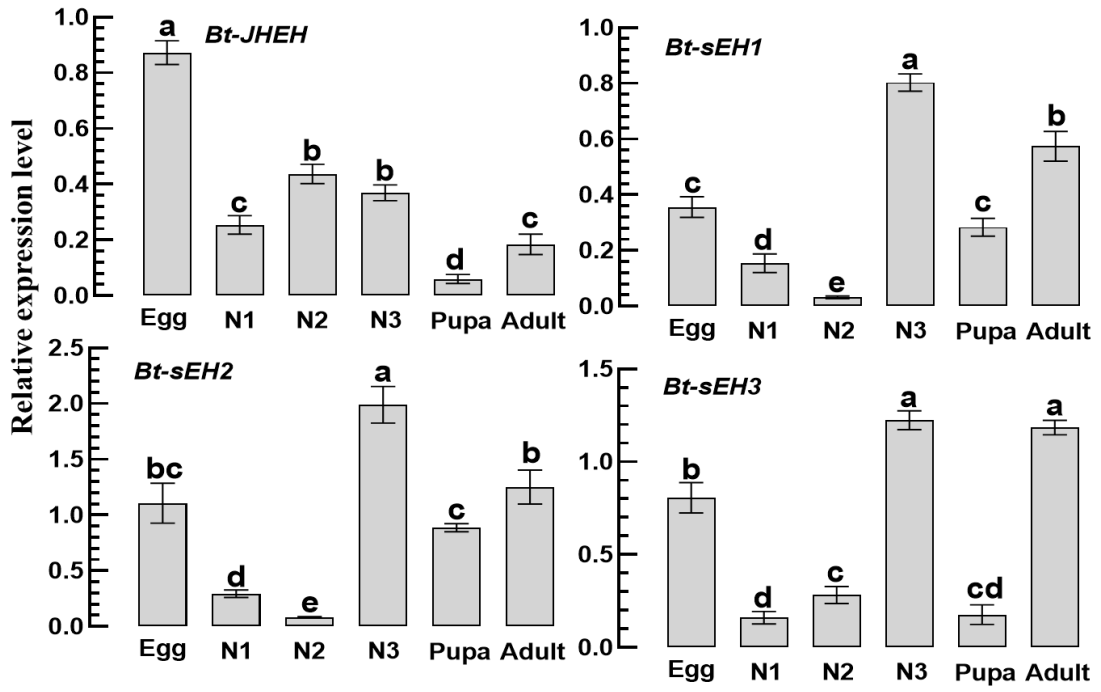

(A)
Rn-CYP1
Mm-CYP1
Mm-CYP5
Hs-CYP1
Mm-CYP3
Mm-CYP2
Hs-CYP3
Hs-CYP4
Hs-CYP5
Mm-CYP4
Hs-CYP2
Bt-CYP7
Bt-CYP6
Fo-CYP24
Se-CYP32
Bt-CYP5
Bt-CYP1
Bt-CYP36
Bt-CYP15
Bt-CYP37
Bt-CYP14
Bt-CYP16
Bt-CYP17
Bt-CYP25
Bt-CYP35
Bt-CYP44
Bt-CYP38
Bt-CYP43
Bt-CYP4
Bt-CYP27
Bt-CYP3
Bt-CYP23
Bt-CYP30
Bt-CYP2
Bt-CYP21
Bt-CYP19
Bt-CYP41
Bt-CYP39
Bt-CYP12
Bt-CYP40
Bt-CYP13
Bt-CYP22
Bt-CYP9
Bt-CYP20
Bt-CYP11
Bt-CYP18
Bt-CYP29
Bt-CYP26
Bt-CYP34
Bt-CYP42
Bt-CYP32
Bt-CYP33
Bt-CYP8
Bt-CYP10
Bt-CYP24
Bt-CYP28
Bt-CYP31
(B)
EpOME synthase
Bt-CYP5
Egg N1 N2 N3 Pupa Adult
Relative expression level
Bt-CYP6
Bt-CYP7
(C)
Non-viruliferous
Viruliferous
Relative expression level
ns
*
ns
Bt-CYP5
Bt-CYP6
Bt-CYP7
(D)
Relative TYLCV titer
dsCON
dsBt-CYP5
dsBt-CYP6
dsBt-CYP7

Fig. 6

**(A)**


sEH
mEH
Bt-EH2
Bt-EH3
Bt-EH1
Ggal
Mmus
sRnor
Spur
Hsap Hs
Fo-EH2
Aaeg PB
Aaeg PA
Bm
Bmor X1
Bmor X2
Pxyl
Harm
Slit
Se-sEH
Bt-JHEH
Agam1
Agam2
Dmel
mRnor
Hsap
mBmori
Fo-JHEH
Se-JHEH
50.00

**(B)**


Relative expression level
Bt-JHEH
Bt-sEH1
Bt-sEH2
Bt-sEH3
Egg
N1
N2
N3
Pupa
Adult

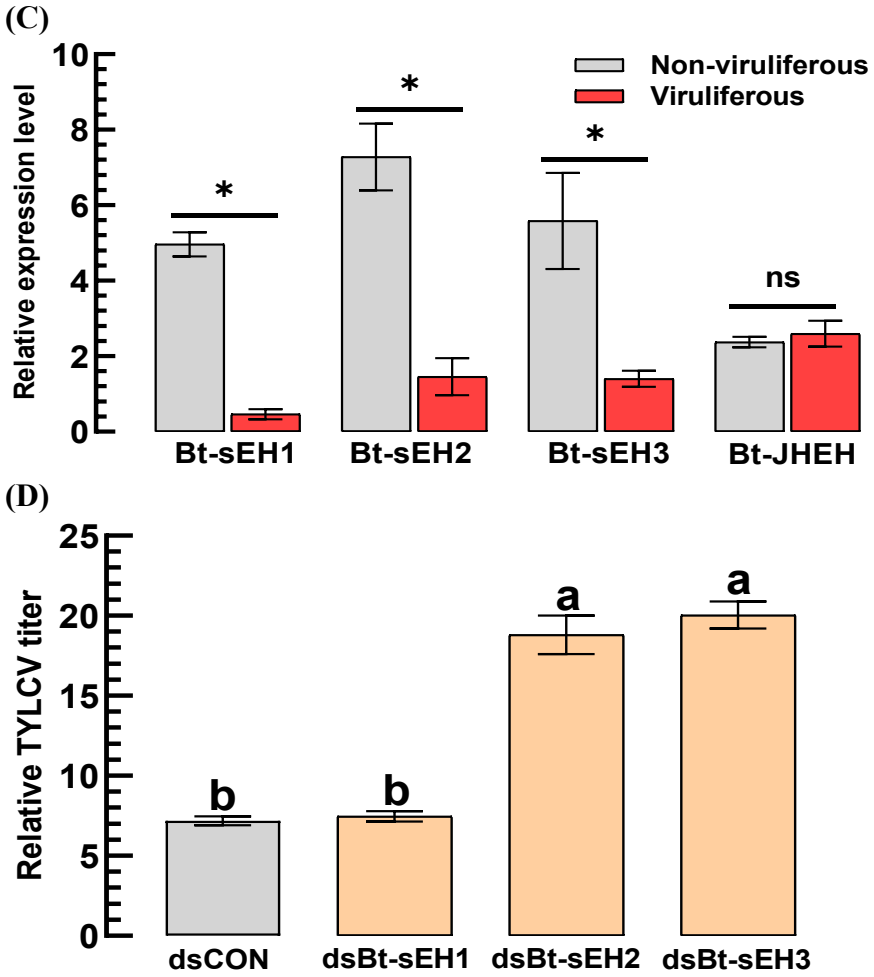

(C)
Relative expression level
10
8
6
4
2
0
Non-viruliferous
Viruliferous
*
*
*
ns
Bt-sEH1
Bt-sEH2
Bt-sEH3
Bt-JHEH
(D)
Relative TYLCV titer
25
20
15
10
5
0
b
b
a
a
dsCON
dsBt-sEH1
dsBt-sEH2
dsBt-sEH3

**Fig. 7**

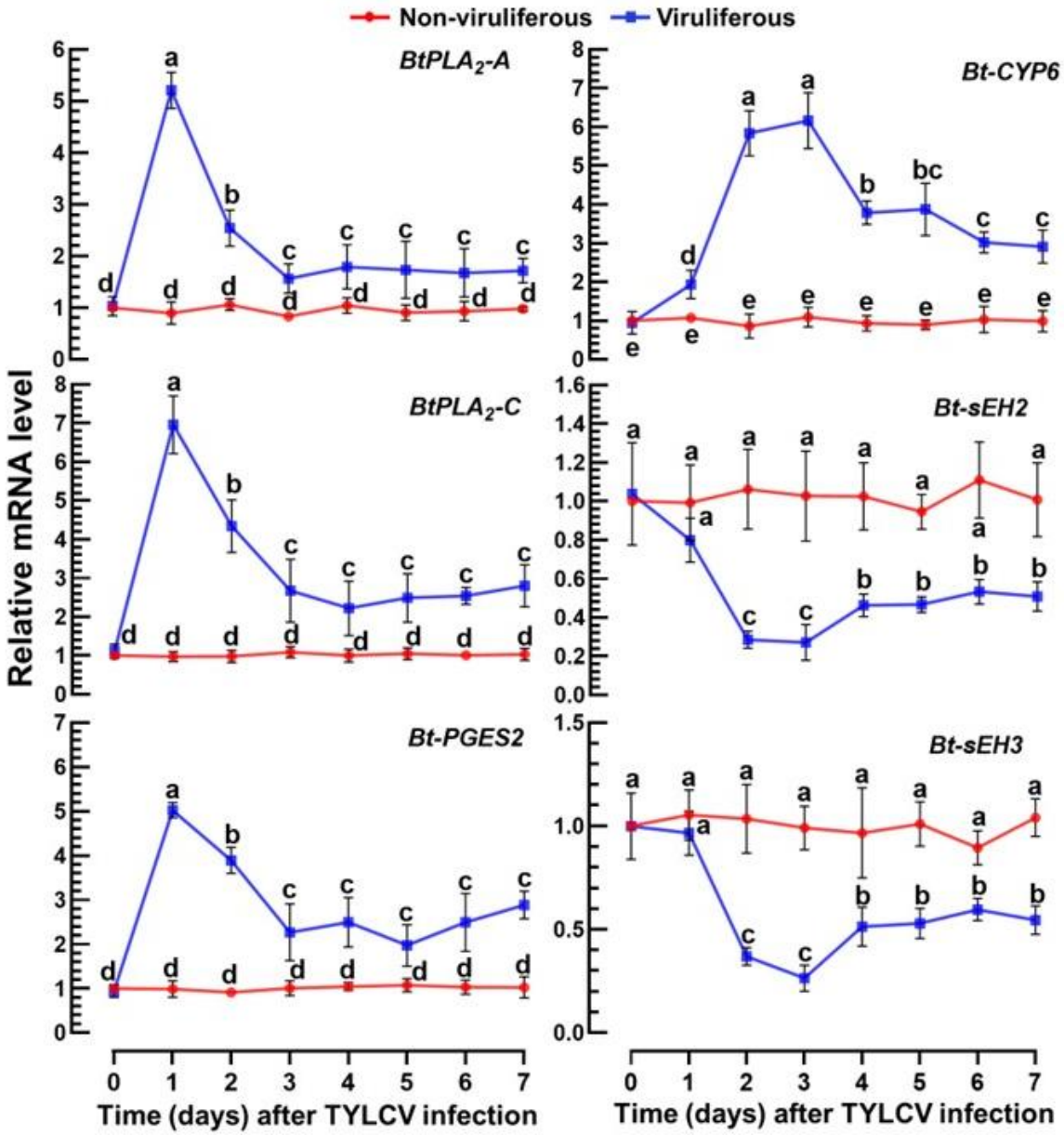
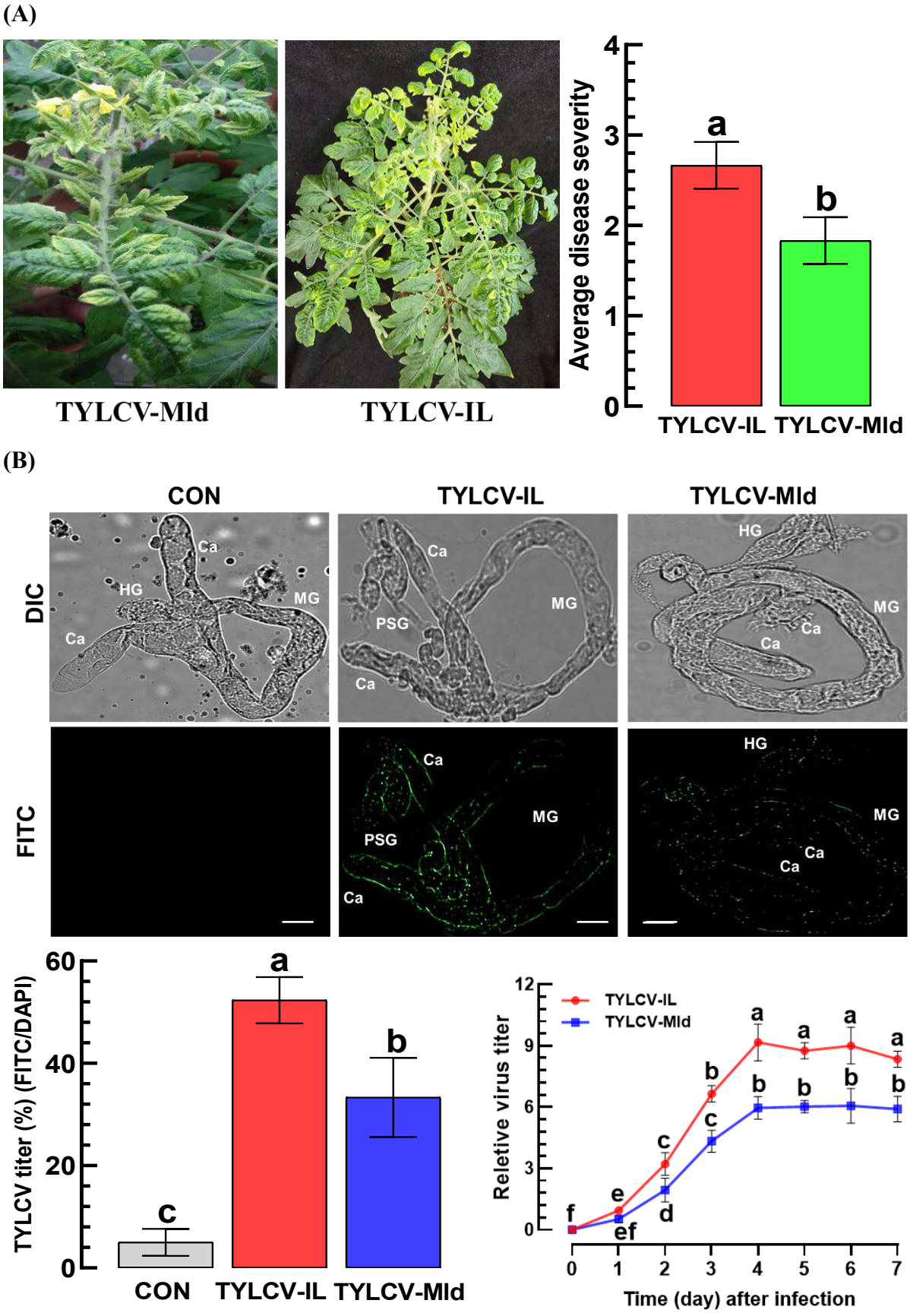

Non-viruliferous
Viruliferous
BtPLA2-A
Bt-CYP6
BtPLA2-C
Bt-sEH2
Bt-PGES2
Bt-sEH3
Relative mRNA level
Time (days) after TYLCV infection
Time (days) after TYLCV infection

**Fig. 8**


(A)
TYLCV-Mld
TYLCV-IL
Average disease severity
a
b
TYLCV-IL
TYLCV-Mld
(B)
CON
TYLCV-IL
TYLCV-Mld
DIC
FITC
Ca
HG
MG
PSG
TYLCV titer (%) (FITC/DAPI)
CON
TYLCV-IL
TYLCV-Mld
Reletive virus titer
Time (day) after infection

(C)

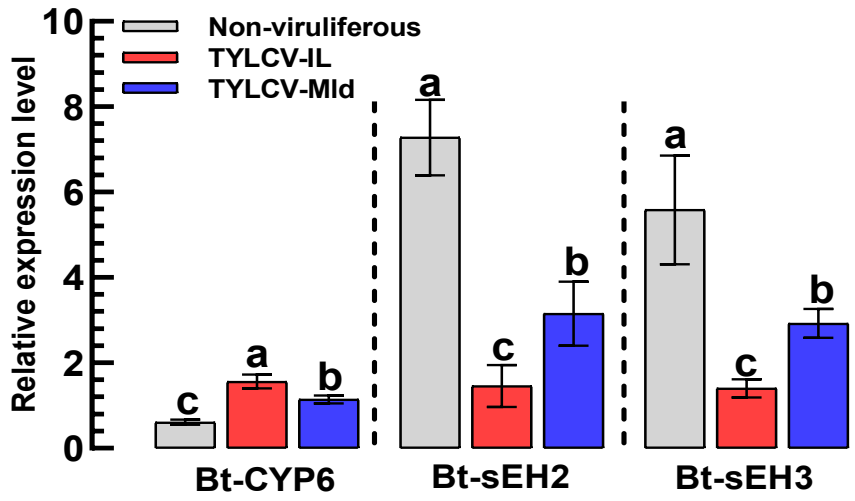
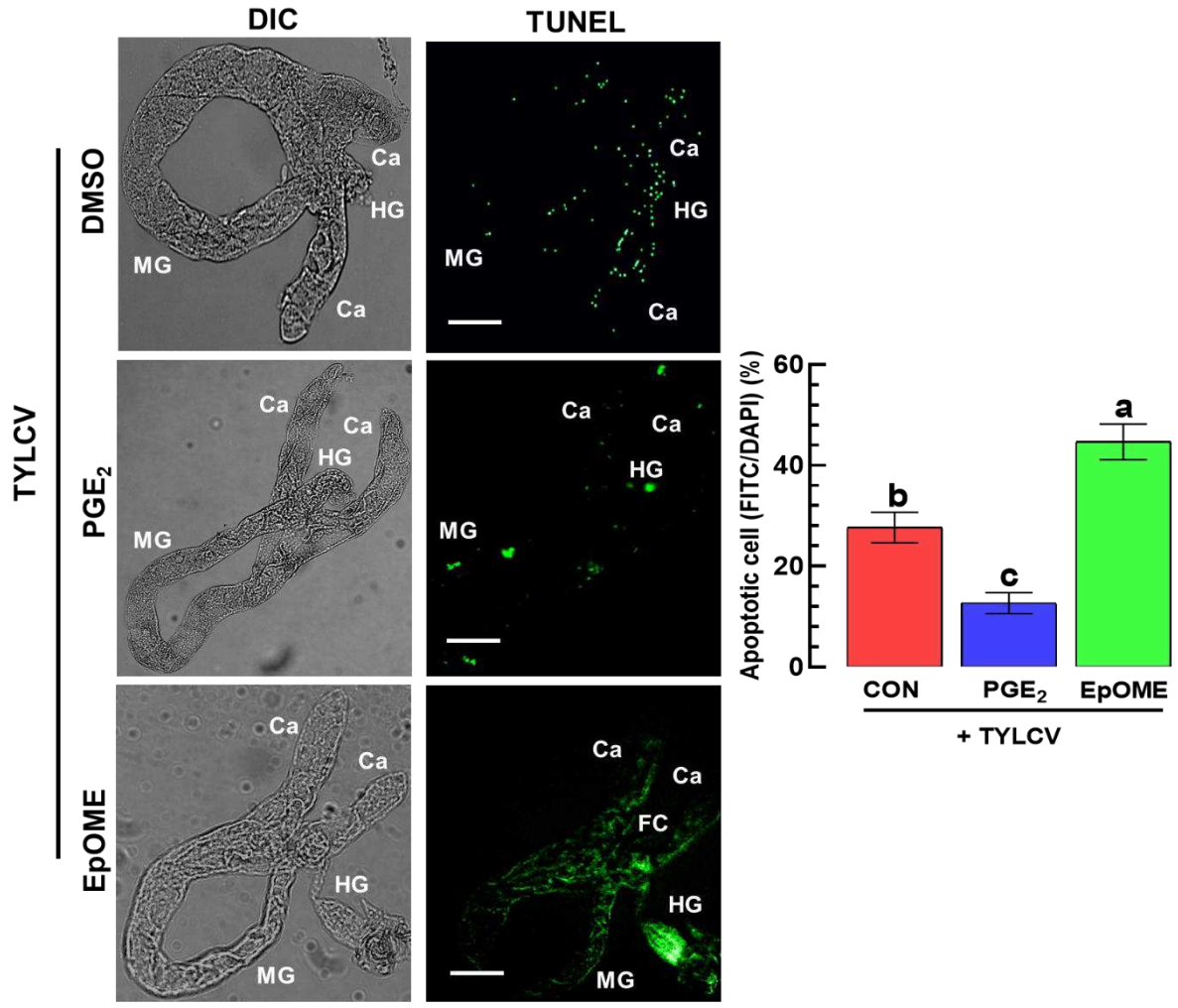
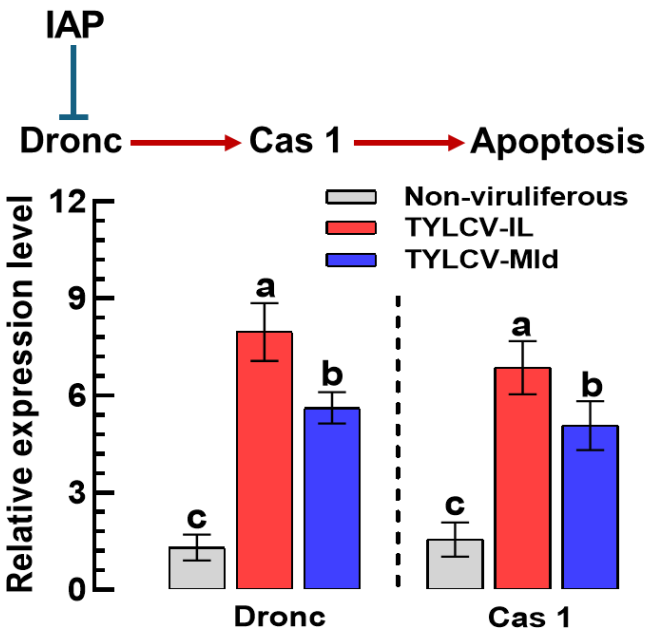

Non-viruliferous
TYLCV-IL
TYLCV-Mld
Relative expression level
10
8
6
4
2
0
a
c
b
a
c
b
a
c
b
Bt-CYP6
Bt-sEH2
Bt-sEH3

**Fig. 9**

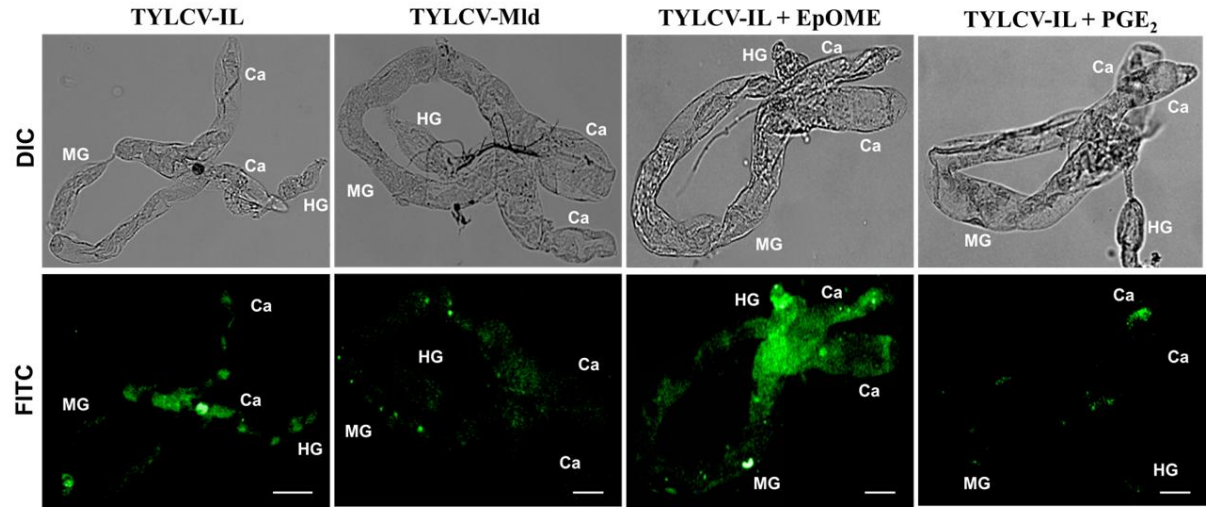
**(A)**


DIC
TUNEL
TYLCV
DMSO
PGE2
EpOME
Ca
HG
MG
FC
Apoptotic cell (FITC/DAPI) (%)
60
40
20
0
a
b
c
CON
PGE2
EpOME
+ TYLCV

**(B)**


IAP
Dronc
Cas 1
Apoptosis
Non-viruliferous
TYLCV-IL
TYLCV-Mld
Relative expression level
12
9
6
3
0
a
b
c
Dronc
Cas 1

(C)


TYLCV-IL
TYLCV-Mld
TYLCV-IL + EpOME
TYLCV-IL + PGE2
DIC
FITC
Ca
MG
HG

(D)

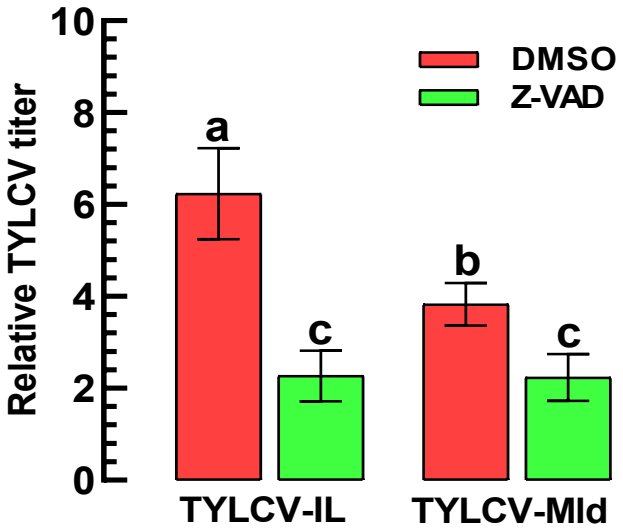

Relative TYLCV titer
10
8
6
4
2
0
DMSO
Z-VAD
a
b
c
c
TYLCV-IL
TYLCV-Mld

**Fig. 10**

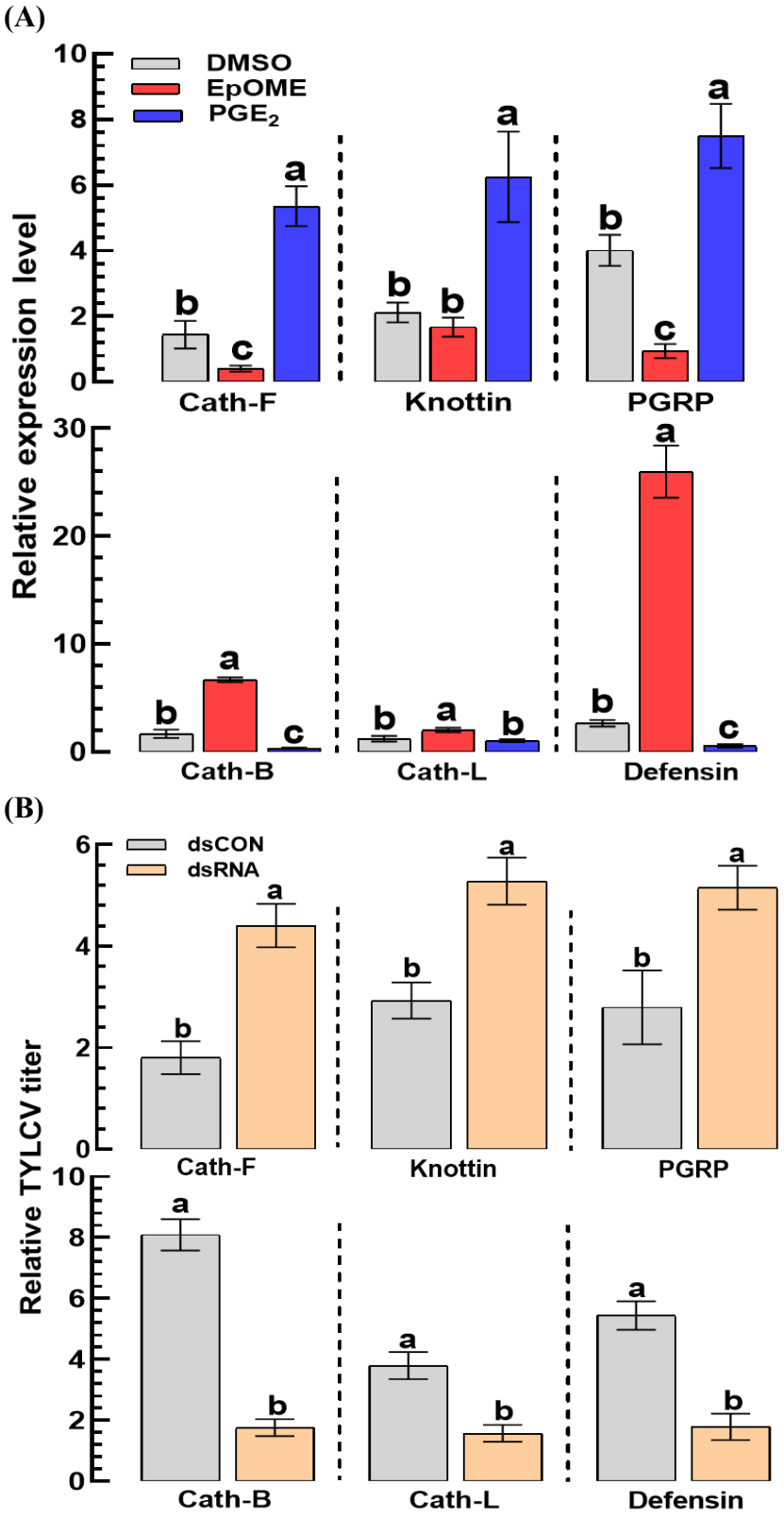
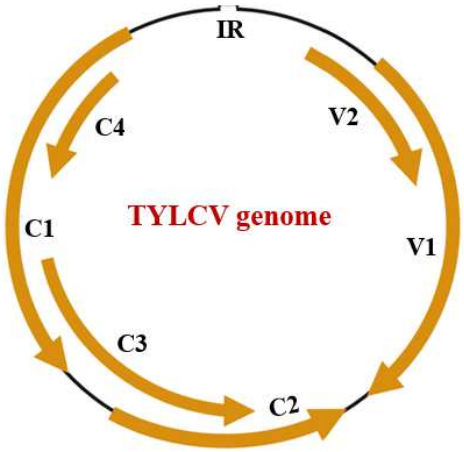
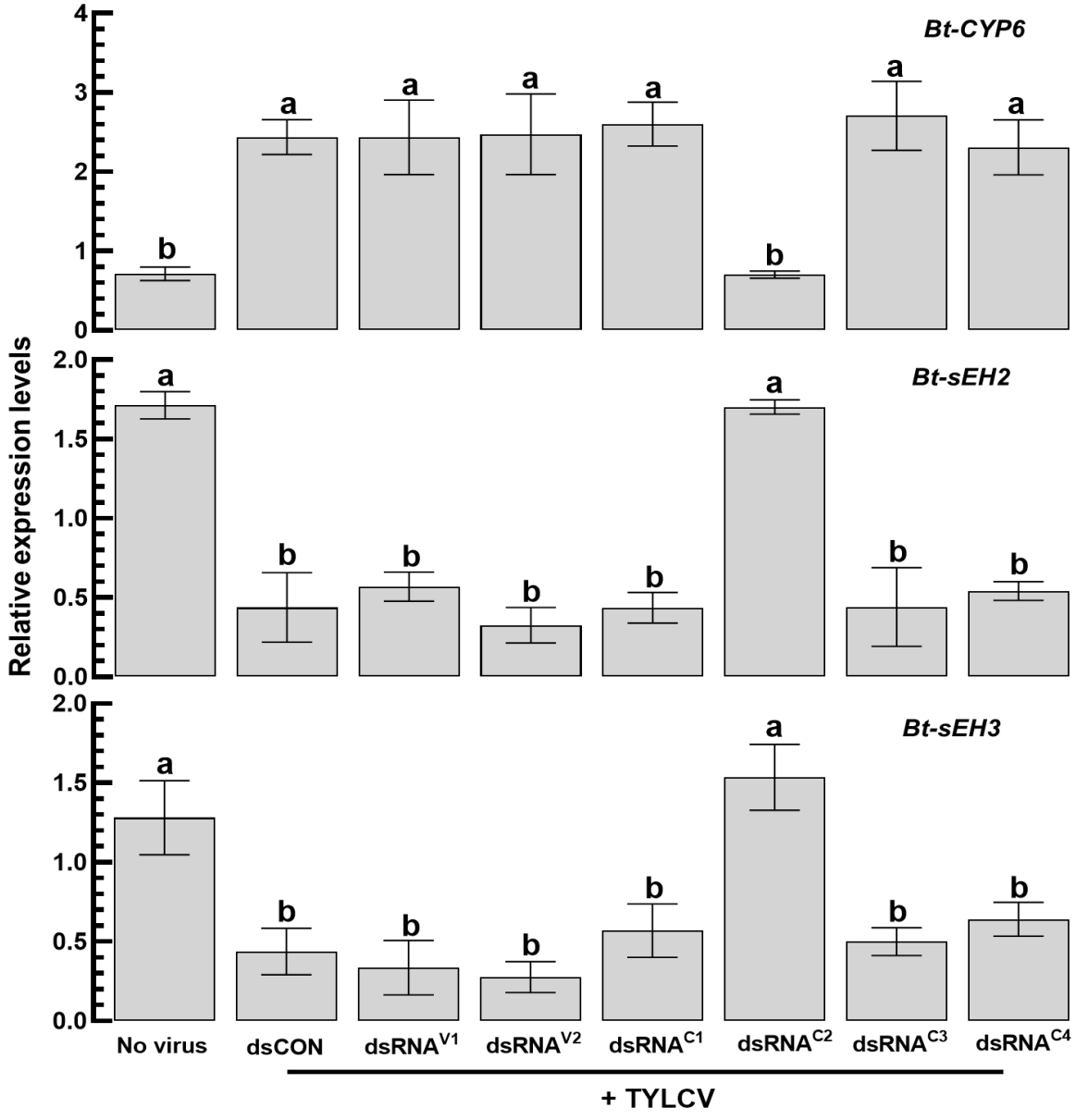

(A)
DMSO
EpOME
PGE2
Relative expression level
Cath-F
Knottin
PGRP
Cath-B
Cath-L
Defensin
(B)
dsCON
dsRNA
Relative TYLCV titer
Cath-F
Knottin
PGRP
Cath-B
Cath-L
Defensin

**Fig. 11**

**(A)**


IR
V2
C4
TYLCV genome
C1
V1
C3
C2

**(B)**


Bt-CYP6
Bt-sEH2
Bt-sEH3
Relative expression levels
No virus
dsCON
dsRNA^V1
dsRNA^V2
dsRNA^C1
dsRNA^C2
dsRNA^C3
dsRNA^C4
+ TYLCV

**(C)**

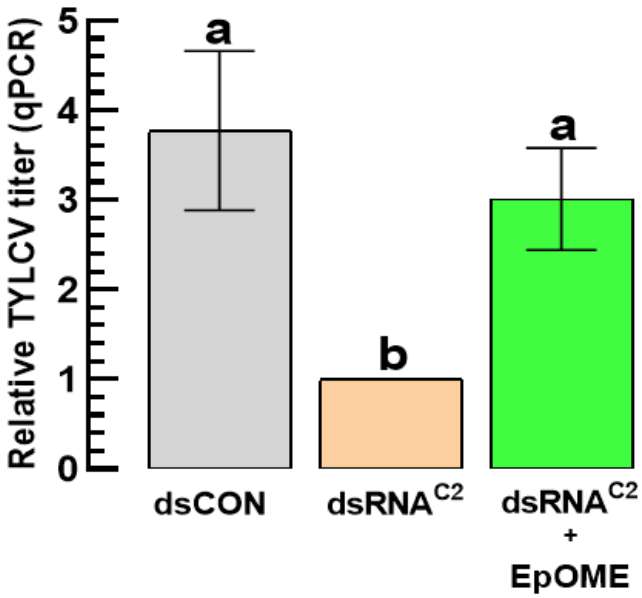

Relative TYLCV titer (qPCR)
0
1
2
3
4
5
a
b
a
dsCON
dsRNA$^{C2}$
dsRNA$^{C2}$
+
EpOME

**Fig. 12**

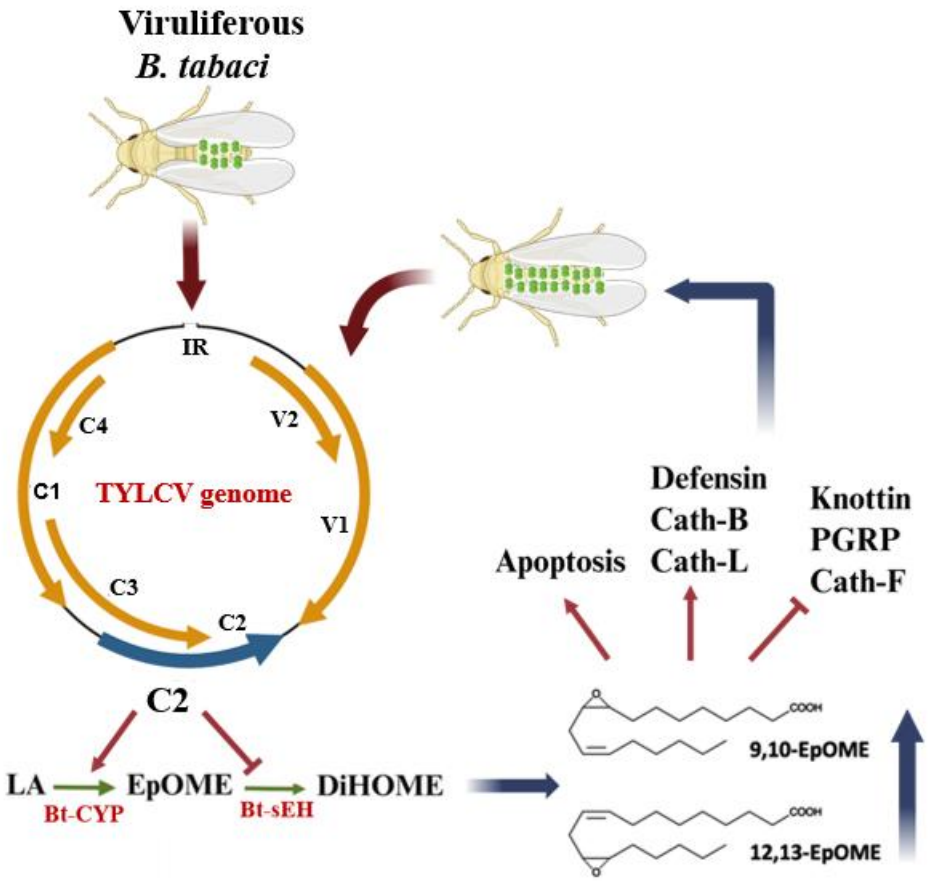

Viruliferous
B. tabaci
IR
C4
V2
C1
TYLCV genome
V1
C3
C2
C2
LA
EpOME
DiHOME
Bt-CYP
Bt-sEH
Apoptosis
Defensin
Cath-B
Cath-L
Knottin
PGRP
Cath-F
9,10-EpOME
12,13-EpOME

**Fig. 13**

## Supplementary Files

This is a list of supplementary files associated with this preprint. Click to download.

- SupplementaryInformation.docx